

# A Model of Venous Return while Utilizing Vacuum Assist during Cardiopulmonary Bypass

By

Scott M. Brown, B.S.

A thesis presented to the faculty of the  
Milwaukee School of Engineering  
in partial fulfillment of the requirements for the  
Degree of Master of Science in Perfusion.

May 17, 2000  
Milwaukee, Wisconsin

## **Abstract**

In order for vacuum assisted venous return to be used safely and efficiently, a full understanding of venous return is necessary. Through the use of the concepts of conservation of energy and viscous energy dissipation, a theoretical model of venous return utilizing vacuum assist has been developed in this work. The effectiveness and accuracy of this model has been verified through *in vitro* laboratory investigations and statistical analysis. In summary, the developed model accurately predicts flow rates given cannula size, amount of vacuum applied, and circuit dimensions. Although vacuum assisted venous return can provide higher flows through smaller cannula, vacuum assist can lead to increased levels of shear stress that the blood is exposed to as well as an increased likelihood of cavitation in the venous line. Both of which may lead to an exacerbation of the detrimental effects of cardiopulmonary bypass.

### Acknowledgments

The author is grateful to his committee for their time and effort put towards this project, especially Dr. Charles S. Tritt. Committee members included:

Academic Advisor: Dr. Charles S. Tritt  
Committee Reader: Dr. Larry Fennigkoh  
Committee Reader: Dr. Ron Gerrits

The author would like to acknowledge the efforts of the following individuals for helping bring all the necessary components of the laboratory investigation together:

Charles Altenbern, B.S., C.C.P.  
Chris Cornell, Agilent Technologies  
Michael Gough, B.S., C.C.P.  
Martin Handley, Manager, Technical Support Center, MSOE  
Nicole M. Michaud, M.S., C.C.P.  
Jennifer Padderud, Medtronic

## Table of Contents

	<u>page</u>
<b>Abstract</b> .....	ii
<b>Introduction</b> .....	1
<b>Background</b> .....	2
The Bernoulli Theorem.....	3
<b>The Head Loss Factor</b> .....	6
Frictional Head Losses along Tubes.....	6
Frictional Head Losses Due to Entrance and Exit Effects.....	8
Frictional Head Losses Due to Sudden Diameter Changes.....	9
Frictional Head Losses Due to Diverging Flow.....	10
Frictional Head Losses Due to Converging Flows.....	12
<b>Venous Line Configurations</b> .....	13
Development of the Detailed Model for the Dual-Stage Cannulation Technique.....	15
Development of the Detailed Model for the Single-Stage Cannulation Technique.....	18
<b>Wall Shear Stress</b> .....	22
Effects of High Shear Stress Levels on Flowing Blood.....	23
<b>Cavitation</b> .....	23
<b>Laboratory Procedure</b> .....	26
Equipment.....	28
<b>Results</b> .....	34
<b>Analysis</b> .....	55
<b>Conclusions</b> .....	59
<b>References</b>	

## List of Figures

	<u>page</u>
<b>Figure 1:</b> Schematic of the diverging flow configuration.....	10
<b>Figure 2:</b> Schematic of the converging flow configuration.....	12
<b>Figure 3:</b> Venous return utilizing a single dual-stage venous cannula.....	14
<b>Figure 4:</b> Venous return utilizing two single-stage venous cannula.....	14
<b>Figure 5:</b> Representation of the factors associated with shear stress.....	22
<b>Figure 6:</b> Circuit configuration used to test the model for the dual-stage venous cannula.....	29
<b>Figure 7:</b> Circuit configuration used to test the model for the single-stage venous cannula.....	30
<b>Figure 8:</b> Graph of the predicted and average measured flows at each level of vacuum for the 28/38 Fr. dual-stage cannula .....	36
<b>Figure 9:</b> Graph of the predicted and average measured flows at each level of vacuum for the 29/29 Fr. dual-stage cannula .....	36
<b>Figure 10:</b> Graph of the predicted and average measured flows at each level of vacuum for the dual 24 Fr. single-stage cannula .....	37
<b>Figure 11:</b> Graph of the predicted and average measured flows at each level of vacuum for the dual 18 Fr. single-stage cannula .....	37
<b>Figure 12:</b> Graph of the predicted and average measured flows at each level of vacuum for the dual 12 Fr. single-stage cannula .....	38
<b>Figure 13:</b> Graph of the predicted and average measured pressure drop at each level of vacuum for the 28/38 Fr. dual-stage cannula.....	41
<b>Figure 14:</b> Graph of the predicted and average measured pressure drop at each level of vacuum for the 29/29 Fr. dual-stage cannula.....	41
<b>Figure 15:</b> Graph of the predicted and average measured pressure drop at varying levels of vacuum for the 24 Fr. single-stage cannula.....	42
<b>Figure 16:</b> Graph of the predicted and average measured pressure drop at each level of vacuum for the 18 Fr. single-stage cannula.....	42

### List of Figures (continued)

	<u>page</u>
<b>Figure 17:</b> Graph of the predicted and average measured pressure drop at each level of vacuum for the 12 Fr. single-stage cannula.....	43
<b>Figure 18:</b> Graph of the predicted and average estimated wall shear stress values for the 28/38 Fr. dual-stage cannula.....	46
<b>Figure 19:</b> Graph of the predicted and average estimated wall shear stress values for the 29/29 Fr. dual-stage cannula.....	46
<b>Figure 20:</b> Graph of the predicted and average estimated wall shear stress values for the 24 Fr. single-stage cannula.....	47
<b>Figure 21:</b> Graph of the predicted and average estimated wall shear stress values for the 18 Fr. single-stage cannula.....	47
<b>Figure 22:</b> Graph of the predicted and average estimated wall shear stress values for the 12 Fr. single-stage cannula.....	48
<b>Figure 23:</b> Graph of the average bubble count per level versus the amount of vacuum applied for the 28/38 Fr. dual-stage cannula.....	51
<b>Figure 24:</b> Graph of the average bubble count per level versus the amount of vacuum applied for the 29/29 Fr. dual-stage cannula.....	52
<b>Figure 25:</b> Graph of the average bubble count per level versus the amount of vacuum applied for the 24 Fr. single-stage cannula.....	52
<b>Figure 26:</b> Graph of the average bubble count per level versus the amount of vacuum applied for the 18 Fr. single-stage cannula.....	53
<b>Figure 27:</b> Graph of the average bubble count per level versus the amount of vacuum applied for the 12 Fr. single-stage cannula.....	53
<b>Figure 28:</b> Graph of measured versus predicted flows for all cannulas tested along with the corresponding regression line.....	55
<b>Figure 29:</b> Graph of the estimated versus predicted cannula wall shear stress values for all cannulas tested along with the corresponding regression line.....	57

## List of Tables

	<u>page</u>
<b>Table 1:</b> Measured dimensions for the dual-stage cannula circuit of Figure 6.....	31
<b>Table 2:</b> Measured dimensions for the single-stage cannula circuit of Figure 7.....	31
<b>Table 3:</b> Predicted and average measured flows for each dual-stage cannula.....	34
<b>Table 4:</b> Predicted and average measured flows for each single-stage cannula.....	35
<b>Table 5:</b> Predicted and average measured pressure drop for each dual-stage cannula.....	39
<b>Table 6:</b> Predicted and average measured pressure drop for each single-stage cannula.....	40
<b>Table 7:</b> Predicted and average estimated values of wall shear stress for each dual-stage cannula.....	44
<b>Table 8:</b> Predicted and average estimated values of wall shear stress for each single-stage cannula.....	45
<b>Table 9:</b> Average bubble counts at each level of vacuum for the 28/38 Fr. dual-stage cannula.....	49
<b>Table 10:</b> Average bubble counts at each level of vacuum for the 29/29 Fr. dual-stage cannula.....	49
<b>Table 11:</b> Average bubble counts at each level of vacuum for the 24 Fr. single-stage cannula.....	50
<b>Table 12:</b> Average bubble counts at each level of vacuum for the 18 Fr. single-stage cannula.....	50
<b>Table 13:</b> Average bubble counts at each level of vacuum for the 12 Fr. single-stage cannula.....	51
<b>Table 14:</b> Average value of the inlet head loss constant for each cannula.....	54

## **List of Appendices**

**Appendix A:** Blood Gas Data

**Appendix B:** Random Number Tables

**Appendix C:** Measured Flow and Cannula Pressure Drop Data for the Dual-Stage Cannulas

**Appendix D:** Measured Flow and Cannula Pressure Drop Data for the Single-Stage Cannulas

**Appendix E:** Measured Bubble Counts for the Dual-Stage and Single-Stage Cannulas

**Appendix F:** Predicted Data from the Model for Each Cannula

**Appendix G:** Statistical Powers for the Analysis of the Bubble Count Data of Each Cannula

**Appendix H:** t-Statistic Calculation for the Comparison of the Model and Measured Data



## **Introduction**

Traditionally, venous return to the cardiectomy reservoir on the heart lung machine has been made possible by creating a siphon in the venous line. Recently, as technology has made it possible to perform minimally invasive heart surgery, the need for less cumbersome cannulation techniques has arisen [1]. In parallel to this is the desire to decrease the hemodilutional effect of cardiopulmonary bypass by miniaturizing the bypass circuit and subsequently decreasing the prime volume [2, 3]. With both these demands being placed on the perfusionist, the advent of utilizing assisted venous return arose. One common form of assisted venous return is accomplished by connecting a vacuum source to the cardiectomy reservoir; hence the name vacuum assisted venous return (VAVR). This technique increases the pressure drop across the venous cannula and lines resulting in higher flows even with smaller cannulas and lines [4, 5]. The venous return rate becomes a function of both the siphon (gravity) and the amount of negative pressure (vacuum) applied. The use of VAVR can also decrease the prime volume requirement for the cardiopulmonary bypass circuit, resulting in decreased hemodilution [2, 3].

The results of using VAVR have not yet been adequately investigated outside of its ability to achieve higher flows through smaller bore venous cannula [6]. Previous studies have all been centered on *in vitro* and *in vivo* measurements done with little or no theoretical analysis. Nor has a good model of venous return been developed which considers the pressure drops and shear forces associated with different venous line configurations. In short, at a superficial level VAVR appears to be a success because

circuit miniaturization is possible while maintaining adequate flow rates. But, on a clinical level the net costs have yet to be thoroughly investigated.

Numerous studies have investigated the effect of shear stress on hemolysis, platelet activation, and complement activation [7, 8, 9, 10]. Each of which can have a significant effect on the hemostasis and post-operative morbidity associated with cardiopulmonary bypass [11, 12]. Yet, the combining of what is known about the effects of shear stress on the formed elements of blood and the use of VAVR has been ignored.

The focus of this paper is to first develop a model of venous return from which the effects of utilizing VAVR can be implied. An *in vitro* laboratory investigation will then be used to verify the validity of the proposed model. The goal is to develop a tool that perfusionists and surgeons can use to make informed decisions regarding when to use VAVR. This work will also lay the foundation for follow-up studies focused on the activation of complement and platelets as well as hemolysis associated with VAVR.

### **Background**

When modeling fluid systems, the amount of detail and the complexity of the model depend greatly on the number of dimensions chosen for the model. The use of either one, two, or three-dimensional modeling is possible [13]. One-dimensional models use the concept of streamline flow in which there is no variation in the velocity or the pressure except for that which occurs along the streamline [13]. However, it is still possible to use one-dimensional modeling of fluid flow through a tube network as long as the streamlines are parallel at the entrance and exit to the tube [14]. For this model, this condition will be assumed.

Two and three-dimensional models result in more complex computations. For this reason, one-dimensional models are often used in more complex cases and the results are still valid. As mentioned previously, the goal of the present work is to provide a model for perfusionists and surgeons to use in their practice; therefore, it is important to keep the model simple. For these reasons, a one-dimensional model is most appropriate.

### The Bernoulli Theorem

There are three fundamental forms of energy associated with the flow of fluids through tubes, one of these being kinetic and two being potential. The kinetic energy is the energy associated with the fluid's velocity,  $V$ . The potential energy is derived from two sources, one being gravity associated with a height,  $Z$ , above some reference point (datum) and the second being pressure,  $P$  [15, 16]. The equation representing the sum of these energies represents one form of what is known as Bernoulli's Theorem as shown in Equation 1[17].

$$E = gZ + \frac{P}{\rho} + \frac{V^2}{2} \quad 1$$

Where  $E$  = total energy at a point,  $g$  = acceleration due to gravity,  $Z$  = height above a reference line,  $P$  = pressure,  $\rho$  = density, and  $V$  = average velocity.

The principle of conservation of energy states that energy can not be created nor destroyed. However, forms of energy can be interconverted [15]. Therefore, between any two points along a tube the expression of Equation 2 must apply [17].

$$E_1 + E_M = E_2 + E_L \quad 2$$

Equation 2 states that the energy at point one ( $E_1$ ) plus any mechanical energy ( $E_M$ ) added must be equal to the energy at point two ( $E_2$ ) plus the energy lost ( $E_L$ ). For the model being developed, there is no mechanical energy input; therefore, the mechanical energy term is dropped. The lost energy term accounts for frictional losses along a tube. These losses occur at entrances, exits, diverging and converging segments, bends, and changes in cross sectional area. These will be described in detail in following sections.

Combining Equations 1 and 2 gives a more common form of the Bernoulli equation [13, 17]:

$$gZ_1 + \frac{P_1}{\rho} + \frac{V_1^2}{2} = gZ_2 + \frac{P_2}{\rho} + \frac{V_2^2}{2} + E_L \quad 3$$

Solving Equation 3 for the pressure drop from point 1 to point 2 results in the following fundamental equation defining the pressure drop along any section of tube, also known as the Bernoulli equation [17, 18]:

$$\Delta P = \rho g(Z_2 - Z_1) + \rho \frac{(V_2^2 - V_1^2)}{2} + E_L \quad 4$$

In Equation 4, the head loss due to friction ( $E_L$ ) is the energy losses between two points. This term is important for the development of this model. It incorporates all the pressure head losses associated with the viscous effects of the fluid (blood in this case), diameter changes, entrance and exit effects, and convergence and divergence of flow. Equation 4 is the form of the Bernoulli equation that will be used in the formation of the model of venous return to the cardiopulmonary bypass circuit and the effects of utilizing VAVR.

At this point, it is important to describe some concepts imperative to the development of the model. First, flow is defined as a volume of fluid moving past a given point per unit of time [19]. The variables that determine flow,  $Q$ , are pressure,  $P$ , and resistance,  $R$ , in the following manner [19]:

$$Q = \frac{\Delta P}{R} \quad 5$$

From Equation 5 it can be concluded that in order for flow to change there must be either a change in pressure drop or a change in resistance. Yet, a closer look at the definition of flow reveals that it is the product of average velocity,  $V$ , and cross-sectional area,  $A$  [15]:

$$Q = V * A \quad 6$$

For a system with constant flow, any change in area must be offset by a change in velocity. Using Equation 6, the relationship between cross-sectional area and velocity for a constant flow system is as shown in Equation 7.

$$V_1 * A_1 = V_2 * A_2 \Rightarrow V_2 = V_1 \left( \frac{A_1}{A_2} \right) \quad 7$$

This point will become important as different diameter tubing is considered.

Next, in order to apply the particular laws to the model, a few assumptions have to be made. First, the blood will be considered to be a Newtonian, incompressible fluid. This is a common assumption required to solve problems involving the flow of blood and is necessary in order to use the equations chosen. Second, it will be assumed that the flow is fully developed at all times therefore neglecting entrance lengths, again this is

another common assumption. Lastly, the system will be assumed to be rigid and closed. This means that the net flow through the system must be constant.

By examining the Bernoulli equation and neglecting the head loss due to friction for a moment, a couple of implications can be made by inspection. An increase in velocity leads to a decrease in pressure and vice versa [15]. This simple concept works well when the viscous effects of a fluid are ignored. But, as mentioned earlier, the viscous effects have an important role in this model due to the viscous nature of blood and the relatively small tubing diameters.

### **The Head Loss Factor**

With the foundation of the model laid out, it is now important to examine the head losses in more detail. This factor is made up of the pressure losses (or gains) which occur along any defined length of tube. The magnitude of this factor depends primarily on the geometry of the tube network combined with the flow conditions (i.e. laminar versus turbulent flow).

As mentioned previously, there are many causes of head loss in fluid flow through a tube. Friction along a tube, in bends, converging and diverging segments, diameter changes, entrances, and exits all contribute the head loss along a tube. Historically, the equations and coefficients that govern the head losses were derived from experimental data.

### **Frictional Head Losses along Tubes**

Frictional head loss along tubes is likely the most significant factor effecting the overall pressure head loss [20]. This term includes the effects of laminar or turbulent flow. Frictional head losses also play a major role in the shear stress experienced by a

fluid flowing through a tube. The general equation for the frictional head loss along a tube is known as the Darcy-Weisbach Equation [17, 18, 21]:

$$h_f = f * \frac{L}{D} * \frac{V^2}{2g} \quad 8$$

As mentioned previous, the frictional head loss depends on whether or not the fluid is in laminar or turbulent flow. The way this is accommodated by Equation 8 is through the dimensionless friction factor,  $f$ .

At this point, it is important to define the conditions for laminar and turbulent flow. Traditionally, the Reynolds number has been the measure of the flow regime. It is defined by Equation 9 [22, 23].

$$\text{Reynolds number, } N_{\text{Re}} = \frac{V * D * \rho}{\mu} \quad 9$$

In Equation 9, the fluid viscosity is denoted as  $\mu$ . The transition from laminar to turbulent flow regimes is generally accepted to occur at 2,300 and will therefore be used for the model being developed [16, 23].

The friction factor for laminar flow was initially determined experimentally by several investigators. The initial investigator, Nikuradse, has been given credit for developing the standard for this measurement. The equations were derived from a family of curves depicting the friction factor versus Reynolds number [13, 24]. In equation format, the friction factor for laminar flow is defined as [13, 17]:

$$f = \frac{64}{N_{\text{Re}}} = \frac{64 * \mu}{V * D * \rho} \quad 10$$

One equation for the friction factor for turbulent flow is [13, 17]:

$$f = \frac{0.316}{(N_{Re})^{0.25}} = \frac{0.316 * \mu^{0.25}}{(V * D * \rho)^{0.25}} \quad 11$$

Substituting the appropriate friction factor equation into Equation 8 gives an estimate of the frictional head loss along a length of tube. It is important to note that the Reynolds number must be known or calculated for the selection of the proper equation.

#### Frictional Head Losses Due to Entrance and Exit Effects

When a fluid is accelerated into a tube opening from a reservoir, there is a conversion of energy from the potential form to the kinetic form. By the same token, the geometry of the entrance has a great effect on magnitude of the amount of energy lost through the tube opening [17]. For instance, small openings result in a greater energy loss than large openings. Therefore, it would be expected that small openings would result in greater pressure drops. Depending on the geometry of the downstream tube, this pressure drop may or may not be reversible.

At an exit of a tube into a reservoir, the opposite occurs. Just before the fluid leaves the tube it has a velocity associated with it; therefore, there is kinetic energy [17]. Once the fluid enters the reservoir the velocity becomes zero; therefore, the kinetic energy must be accounted for in some form. The result is that the kinetic energy is converted into a potential energy in the form of pressure in combination with a portion of the head being lost to the exit effects.

In either situation, the equation for the calculation of the head loss due to an exit or entrance is given in Equation 12 [17, 18].



$$h_{entrance/exit} = K_L \frac{(V_1 - V_2)^2}{2g} \quad 12$$

The head loss constant,  $K_L$ , has been derived by some investigators as well as determined experimentally by others [17, 18]. The tips of venous cannulas are unique when compared to the inlets to tubes of previous studies. For this reason, the value of  $K_L$  used in the calculation of the head loss due to the cannula entrance will be determined from experimental data for each cannula.

The velocity  $V_1$  is that which the upstream fluid is experiencing and  $V_2$  is that of the down stream fluid. For an entrance, if the fluid was in a reservoir of infinite area,  $V_1$  would be considered zero. But, because the model being developed is for the human body, this is not the case. The fluid must have some initial velocity,  $V_1$ , before it enters through the venous line through the venous cannula. Therefore, the velocity  $V_1$  will be determined by the area of the vessel, either the superior or the inferior vena cava, and the flow through the system as outlined by Equation 6.

For the head loss at an exit, it is the velocity  $V_2$  that is typically assumed to be zero. As the fluid leaves the tubing it is collected in the reservoir and the assumption that the velocity is zero in the reservoir is valid [17]. Therefore, the equation for the head loss due to exit effects becomes:

$$h_{exit} = K_L \frac{V^2}{2g} \quad 13$$

#### Frictional Head Losses Due to Sudden Diameter Changes

The equation for calculating the head loss due to sudden diameter changes is identical to Equation 12. The difference being in the head loss constant,  $K_L$  [17].

$$h_{L/\Delta D} = K_L \frac{(V_1 - V_2)^2}{2g} \quad 14$$

In general, the value of  $K_L$  for a change in diameter is dependent on the ratio of the areas as well as the nature of the contraction or enlargement (either gradual or abrupt). Values of  $K_L$  for diameter changes have been derived through experimentation and theory and are reported in graphical form by several authors [14, 17, 18]. The need to account for the head loss due to sudden changes in diameter will depend on the configuration of the venous line being investigated.

#### Frictional Head Losses Due to Diverging Flow

When a fluid that is flowing in a single tube meets a bifurcation, there is a loss of pressure head as the fluid is forced to separate. The degree or significance of the head loss depends on the diameter of the tubes into which the fluid will be separating as well as the diameter of the feed tube [14, 18]. But, it also is greatly affected by the angle of the bifurcating tube [14]. The greater this angle, the greater will be the head loss. In the models being developed, the separation of flow is depicted in Figure 1.

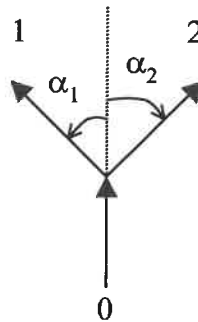


**Figure 1:** Schematic of the diverging flow configuration.

With respect to the model for venous return, the diverging angles  $\alpha_1$  and  $\alpha_2$  are equal; therefore, they will be known simply as  $\alpha$ .

The calculation of the head loss for diverging flow is more complicated than those defined previously. The equation for the head loss from point 0 to 1 is similar to Equations 12 and 14 [18]:

$$h_{div/0,1} = K_{0,1} \frac{(V_0 - V_1)^2}{2g} \quad 15$$

The equation is the same for the flow from point 0 to point 2, just substitute the subscript 2 in for the subscript 1:

$$h_{div/0,2} = K_{0,2} \frac{(V_0 - V_2)^2}{2g} \quad 16$$

The calculation of the head loss constants ( $K_{0,1}$ ,  $K_{0,2}$ ) are shown in Equations 17 and 18 [14]:

$$K_{0,1} = \lambda_1 + (2\lambda_2 - \lambda_1) \left( \frac{V_1}{V_0} \right)^2 - 2\lambda_2 \left( \frac{V_1}{V_0} \right) \cos \alpha' \quad 17$$

$$K_{0,2} = \lambda_1 + (2\lambda_2 - \lambda_1) \left( \frac{V_2}{V_0} \right)^2 - 2\lambda_2 \left( \frac{V_2}{V_0} \right) \cos \alpha' \quad 18$$

Where  $\lambda_1 = 0.0712\alpha^{0.7041} + 0.37$  for  $\alpha < 22.5^\circ$ ,  $\lambda_1 = 1.0$  for  $\alpha \geq 22.5^\circ$ ,  $\lambda_2 = 0.0592\alpha^{0.7029} + 0.37$  for  $\alpha < 22.5^\circ$ ,  $\lambda_2 = 0.9$  for  $\alpha \geq 22.5^\circ$ , and  $\alpha' = 1.41\alpha - 0.00594\alpha^2$ .

Combining Equations 17 and 18 with Equations 15 and 16, respectively, gives the total head loss of the flow separation from point 0 to points 1 and 2.

### Head Losses Due to Converging Flows

Much like the diverging flow situation, the calculation of the head loss due to converging flow is more complex than those defined previously. Converging flow can have a significant effect on the pressure drop through a tubing network due to the collision of particles and the imparting of their energy on surrounding particles.

The schematic for converging flows is shown in Figure 2.

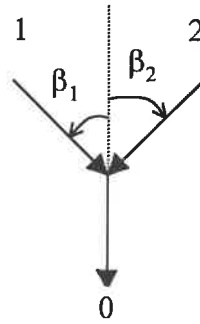


**Figure 2:** Schematic of the converging flow configuration.

As done with diverging flow, the angles  $\beta_1$  and  $\beta_2$  will be equal and will therefore be known simply as  $\beta$ .

The equation for calculating the head loss due to the converging flow from points 1 to 0 is similar to that used for diverging flow [18]:

$$h_{con/1,0} = K_{1,0} \frac{(V_1 - V_0)^2}{2g} \quad 19$$

The equation is the same for the flow from point 2 to point 0, just substitute the subscript 2 in for the subscript 1:

$$h_{con/2,0} = K_{2,0} \frac{(V_2 - V_0)^2}{2g} \quad 20$$

The calculation of the head loss constants ( $K_{1,0}$ ,  $K_{2,0}$ ) is shown in Equations 21 and 22 [14].

$$K_{1,0} = \lambda_3 \left( \frac{V_1}{V_0} \right)^2 + 1 - 2 \left[ \left( \frac{V_1}{V_0} \right) \left( \frac{Q_1}{Q_0} \right) \cos \beta'_1 + \left( \frac{V_2}{V_0} \right) \left( \frac{Q_2}{Q_0} \right) \cos \beta'_2 \right] \quad 21$$

$$K_{2,0} = \lambda_3 \left( \frac{V_2}{V_0} \right)^2 + 1 - 2 \left[ \left( \frac{V_2}{V_0} \right) \left( \frac{Q_2}{Q_0} \right) \cos \beta'_2 + \left( \frac{V_1}{V_0} \right) \left( \frac{Q_1}{Q_0} \right) \cos \beta'_1 \right] \quad 22$$

Where  $\beta'_1 = 1.41\beta_1 - 0.00594\beta_1^2$  and  $\beta'_2 = 1.41\beta_2 - 0.00594\beta_2^2$ .

But, as mentioned previously,  $\beta_1$  and  $\beta_2$  are equal, therefore:

$$\beta' = 1.41\beta - 0.00594\beta^2$$

The constant  $\lambda_3$  has been determined experimentally by researchers and is typically depicted graphically [14]. A typical value of  $\lambda_3$  for a angle  $\beta$  less than  $45^\circ$  is approximately 0.96. There is no algebraic equation for this value.

### **Venous Line Configurations**

With all the pertinent equations for head losses defined, the next step is to define venous line configurations that will be considered for the model. The two methods of cannulation for venous return to the cardiopulmonary bypass circuit are using a single dual-stage cannula or using two single-stage cannulas. The configurations are shown in the Figures 3 and 4.

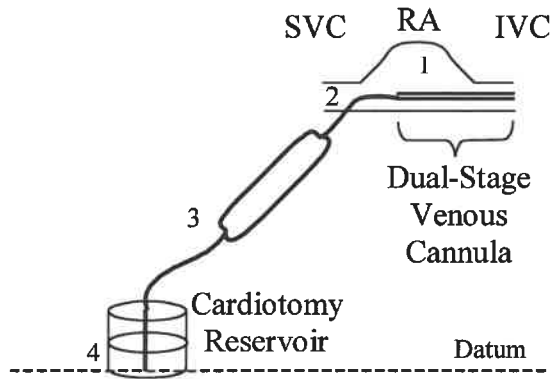


**Figure 3:** Venous return utilizing a single dual-stage venous cannula.

In Figure 3, point 1 refers to the right atrium, point 2 refers to the connection of the cannula to the venous line, point 3 refers to the connection of the venous line to the cardiotomy inlet, and point 4 refers to the level of the outlet from the venous line into the cardiotomy reservoir.

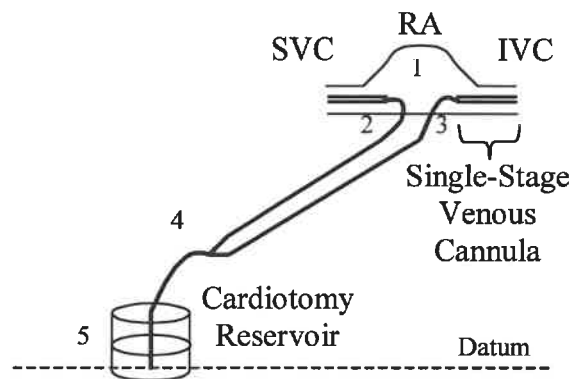


**Figure 4:** Venous return utilizing two single-stage venous cannula.

In Figure 4, point 1 refers to the right atrium, point 2 refers to the connection between the superior vena cava cannula and the venous line, point 3 refers to the

connection between the inferior vena cava cannula and the venous line, point 4 refers to the junction of the superior and inferior vena cava venous lines, and point 5 refers to the level of the outlet from the venous line into the cardiectomy reservoir.

The basis for these models, as mentioned previously, is Bernoulli's energy balance equation as defined in Equation 3. There is an initial amount of energy associated with the blood's velocity before it enters the venous cannula from the superior vena cava (SVC), inferior vena cava (IVC), or the right atrium (RA). As the blood flows in through the venous cannula(s) and through the venous line(s), energy is lost, but these losses can be accounted for utilizing the head loss equations defined earlier. By using these equations it is possible to determine flow rates expected for various combinations of cannula(s), tubing diameters, heights, and applied vacuum.

#### Development of the Detailed Model for the Dual-Stage Cannulation Technique

Beginning with the configuration where a single dual-stage venous cannula is used, as shown in Figure 3, the model starts with a basic statement of the energy balance equation given in Equation 2:

$$E_1 = E_2 + E_{L/1,2} \quad 23$$

$$E_2 = E_3 + E_{L/2,3} \quad 24$$

$$E_3 = E_4 + E_{L/3,4} \quad 25$$

Where:

$$E_{L/1,2} = h_{in} + h_{f/1,2} \quad 26$$

$$E_{L/2,3} = 2 * h_{f/2,3} + h_{diverging\ flow} + h_{converging\ flow} \quad 27$$

$$E_{L/3,4} = h_{f/3,4} + h_{exit} \quad 28$$

Converting Equations 26 through 28 into the format of Equation 3 gives:

$$gZ_1 + \frac{P_1}{\rho} + \frac{V_1^2}{2} = gZ_2 + \frac{P_2}{\rho} + \frac{V_2^2}{2} + E_{L/1,2} \quad 29$$

$$gZ_2 + \frac{P_2}{\rho} + \frac{V_2^2}{2} = gZ_3 + \frac{P_3}{\rho} + \frac{V_3^2}{2} + E_{L/2,3} \quad 30$$

$$gZ_3 + \frac{P_3}{\rho} + \frac{V_3^2}{2} = gZ_4 + \frac{P_4}{\rho} + \frac{V_4^2}{2} + E_{L/3,4} \quad 31$$

Solving Equation 29 for  $P_1$ , Equation 30 for  $P_2$ , and Equation 31 for  $P_3$  gives:

$$P_1 = \rho g(Z_2 - Z_1) + P_2 + \frac{\rho(V_2^2 - V_1^2)}{2} + \rho E_{L/1,2} \quad 32$$

$$P_2 = \rho g(Z_3 - Z_2) + P_3 + \frac{\rho(V_3^2 - V_2^2)}{2} + \rho E_{L/2,3} \quad 33$$

$$P_3 = \rho g(Z_4 - Z_3) + P_4 + \frac{\rho(V_4^2 - V_3^2)}{2} + \rho E_{L/3,4} \quad 34$$

Knowing that the pressure  $P_4$  is found in the fluid at the level of outlet of the venous return into the cardiectomy reservoir, it can be assumed that the pressure at that point, using Bernoulli's principle, is equal to:

$$P_4 = \rho gZ_c + P_c \quad 35$$

Where  $P_c$  is equal to the pressure in the cardiectomy and  $Z_c$  is the height of the fluid column above the outlet of the venous line into the cardiectomy reservoir (datum). The



velocity  $V_4$  is zero, as mentioned previously, because it is assumed that there is no velocity associated with the fluid while it is in the reservoir. The reference line, or datum, is set at the outlet of the venous return into the cardiectomy; therefore,  $Z_4$  is also zero. By making these substitutions along with Equation 35 into Equation 34 a solution for  $P_3$  in terms of  $P_C$  is obtained. Substituting this equation for  $P_3$  into that for  $P_2$  (Equation 33), the equation for  $P_2$  into that for  $P_1$  (Equation 32), and the specific weight,  $\gamma$ , in for  $\rho g$ , all three pressures have solutions in terms of the cardiectomy pressure.

$$P_1 = P_C + \gamma \left( Z_C - Z_1 - \frac{V_1^2}{2g} + h_{f/3,4} + h_{exit} + h_{div.flow} + 2 * h_{f2,3} + h_{con.flow} + h_{entrance} + h_{f/1,2} \right) \quad 36$$

$$P_2 = P_C + \gamma \left( Z_C - Z_2 - \frac{V_2^2}{2g} + h_{f/3,4} + h_{exit} + h_{div.flow} + 2 * h_{f2,3} + h_{con.flow} \right) \quad 37$$

$$P_3 = P_C + \gamma \left( Z_C - Z_3 - \frac{V_3^2}{2g} + h_{f/3,4} + h_{exit} \right) \quad 38$$

Equations 35 through 38 can be used to determine what type of pressure drops would be associated with each section of venous line shown in Figure 3. A convenient way to use this model would be to use a spreadsheet; in this work Quattro Pro was used. Solving Equation 36 for the flow with the pressure  $P_1$  set to zero will give the theoretically obtainable flow that will allow for complete drainage of the SVC, IVC, and RA. The reason for setting  $P_1$  to zero is that while on cardiopulmonary bypass, complete draining of the right side of the heart would result in a pressure of zero, or possibly slightly negative depending on the siphon, or combination of siphon and vacuum, drainage. Therefore, components (i.e. cannula) would be chosen in a manner that would

yield complete drainage of the right atrium, thus the goal would be to achieve a  $P_1$  pressure of 0 mmHg.

Quattro Pro, using an iterative method, will solve for the flow given all the cannula and tubing dimensions, heights, and the pressure of the cardiectomy,  $P_C$ . This pressure is zero or atmospheric when no vacuum is applied. As vacuum is applied, the value of  $P_C$  is the amount of negative pressure applied.

#### Development of the Detailed Model for the Single-Stage Cannulation Technique

Just as was done for the dual-stage cannulation technique, the single-stage cannulation model begins with the basic energy balance equations. But, because there are two separate cannulas, each needs their own set of equations as shown below:

$$E_{SVC} = E_2 + E_{L/SVC,2} \quad 39$$

$$E_{IVC} = E_3 + E_{L/IVC,3} \quad 40$$

$$E_2 = E_4 + E_{L/2,4} \quad 41$$

$$E_3 = E_4 + E_{L/3,4} \quad 42$$

$$E_4 = E_5 + E_{L/4,5} \quad 43$$

Where:

$$E_{L/IVC} = h_{entrance,IVC} + h_{bend,IVC} + h_{f/IVC\ cannula} \quad 44$$

$$E_{L/SVC,2} = h_{entrance,SVC} + h_{bend,SVC} + h_{f/SVC\ cannula} \quad 45$$

$$E_{L/2,4} = h_{f/SVC\ line} + h_{converging\ flows/2,4} \quad 46$$

$$E_{L/3,4} = h_{f/IVC\ line} + h_{converging\ flows/3,4} \quad 47$$

$$E_{L/4,5} = h_{f/4,5} + h_{exit} \quad 48$$

Converting Equations 39 through 43 into the format of Equation 3 gives:

$$gZ_{SVC} + \frac{P_{SVC}}{\rho} + \frac{V_{SVC}^2}{2} = gZ_2 + \frac{P_2}{\rho} + \frac{V_2^2}{2} + E_{L/SVC,2} \quad 49$$

$$gZ_{IVC} + \frac{P_{IVC}}{\rho} + \frac{V_{IVC}^2}{2} = gZ_3 + \frac{P_3}{\rho} + \frac{V_3^2}{2} + E_{L/IVC,3} \quad 50$$

$$gZ_2 + \frac{P_2}{\rho} + \frac{V_2^2}{2} = gZ_4 + \frac{P_4}{\rho} + \frac{V_4^2}{2} + E_{L/2,4} \quad 51$$

$$gZ_3 + \frac{P_3}{\rho} + \frac{V_3^2}{2} = gZ_4 + \frac{P_4}{\rho} + \frac{V_4^2}{2} + E_{L/3,4} \quad 52$$

$$gZ_4 + \frac{P_4}{\rho} + \frac{V_4^2}{2} = gZ_5 + \frac{P_5}{\rho} + \frac{V_5^2}{2} + E_{L/4,5} \quad 53$$

Solving Equation 49 for  $P_{SVC}$ , Equation 50 for  $P_{IVC}$ , Equation 51 for  $P_2$ , Equation 52 for  $P_3$ , and Equation 53 for  $P_4$  yields:

$$P_{SVC} = \rho g(Z_2 - Z_{SVC}) + P_2 + \frac{\rho(V_2^2 - V_{SVC}^2)}{2} + \rho E_{L/SVC,2} \quad 54$$

$$P_{IVC} = \rho g(Z_3 - Z_{IVC}) + P_3 + \frac{\rho(V_3^2 - V_{IVC}^2)}{2} + \rho E_{L/IVC,3} \quad 55$$

$$P_2 = \rho g(Z_4 - Z_2) + P_4 + \frac{\rho(V_4^2 - V_2^2)}{2} + \rho E_{L/2,4} \quad 56$$

$$P_3 = \rho g(Z_4 - Z_3) + P_4 + \frac{\rho(V_4^2 - V_3^2)}{2} + \rho E_{L/3,4} \quad 57$$

$$P_4 = \rho g(Z_5 - Z_4) + P_5 + \frac{\rho(V_5^2 - V_4^2)}{2} + \rho E_{L/4,5} \quad 58$$

As was the case in the dual-stage cannulation model, the pressure at the level of the outlet from the venous line into the cardiectomy reservoir,  $P_5$  in this case, depends on the hydrostatic pressure head from the fluid column above. This pressure can be calculated using the following formula derivable from the Bernoulli equation:

$$P_5 = \rho g Z_C + P_C \quad 59$$

As was the case with the dual-stage cannula model,  $P_C$  is equal to the pressure in the cardiectomy and  $Z_C$  is the height of the fluid column above the outlet of the venous line into the cardiectomy reservoir (datum). The velocity of the fluid in the cardiectomy reservoir is zero; therefore,  $V_5$  is zero. Also, because the height  $Z_5$  is set at the reference line, or datum, this value is also zero. Making these substitutions along with Equation 59 into Equation 58, a solution for  $P_4$  in terms of  $P_C$  is obtained. Substituting the new equation for  $P_4$  into that for  $P_3$  (Equation 57) and  $P_2$  (Equation 56), solutions for both  $P_3$  and  $P_2$  in terms of  $P_C$  are obtained. Finally, substituting the equation for  $P_3$  into that for  $P_{IVC}$  (Equation 55) and substituting the equation for  $P_2$  into that for  $P_{SVC}$  (Equation 54) gives equations for  $P_{IVC}$  and  $P_{SVC}$  in terms of  $P_C$ . The results are shown in the equations below with the specific weight,  $\gamma$ , substituted in for  $\rho g$ :

$$P_{SVC} = P_C + \gamma \left( Z_C - Z_{SVC} - \frac{V_{SVC}^2}{2g} + h_{f/4,5} + h_{exit} + h_{f/SVC\ line} + h_{con.\ flow/3,4} + h_{ent.,SVC} + h_{f/SVC\ cannula} \right) \quad 60$$

$$P_{IVC} = P_C + \gamma \left( Z_C - Z_{IVC} - \frac{V_{IVC}^2}{2g} + h_{f/4,5} + h_{exit} + h_{f/IVC\ line} + h_{con.\ flow/2,4} + h_{ent.,IVC} + h_{f/IVC\ cannula} \right) \quad 61$$

$$P_2 = P_C + \gamma \left( Z_C - Z_2 - \frac{V_2^2}{2g} + h_{f/4,5} + h_{exit} + h_{f/SVC\ line} + h_{con.\ flow/2,4} \right) \quad 62$$

$$P_3 = P_C + \gamma \left( Z_C - Z_3 - \frac{V_3^2}{2g} + h_{f/4,5} + h_{exit} + h_{f/IVC\ line} + h_{con.\ flow/3,4} \right) \quad 63$$

$$P_4 = P_C + \gamma \left( Z_C - Z_4 - \frac{V_4^2}{2g} + h_{f/4,5} + h_{out} \right) \quad 64$$

Equations 59 through 64 can be used to characterize the pressures and the pressure drops associated with each cannula and section of venous line used in the case of bi-caval cannulation.

The easiest way to use the model for equipment selection for cardiopulmonary bypass would be similar to the case of the dual-stage cannulation technique. A spreadsheet such as Quattro Pro could be used to solve Equations 59 through 64. The geometric parameters such as cannula sizes, lengths and heights could then be entered into the spreadsheet. With optimal drainage, the pressure in the superior and inferior vena cava will become zero. Therefore, the best approach to solving the problem would be to set the pressures of the superior and inferior cava ( $P_{SVC}$  and  $P_{IVC}$ , Equations 60 and 61) to zero and solve for flow. This will lead to optimal drainage of both vessels.

When using this model for *in vivo* analysis, two assumptions are necessary. First, it should be assumed that that approximately two-thirds of the circulating blood volume of a patient returns to the right side of the heart via the inferior vena cava whereas one-third of the circulating blood volume returns to the right heart via the superior vena cava. Second, an appropriate ratio between the superior and inferior vena cava cross sectional areas must be determined. This is necessary for the proper conversion of flow to velocity in each vessel.

Once the proper values are entered, Quattro Pro will use an iterative method as done in the case of the dual-stage cannula, to solve for the flow. The independent variable will be the cardiectomy pressure,  $P_C$ , which is zero (atmospheric) when no

vacuum is applied. As vacuum is added, the cardiotomy pressure becomes the amount of applied vacuum.

### **Wall Shear Stress**

The shear stress is a function of the viscosity and the shear rate of the fluid flowing through a tube network. The viscosity is the internal friction or resistance of fluid to flow. With respect to the level of shear stress for a cylindrical geometry similar to that of Figure 5, Equation 65 is commonly used [17, 25]:

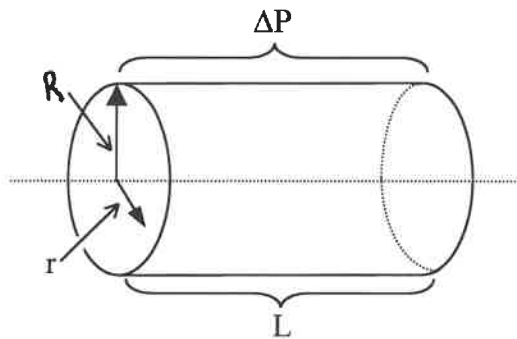


**Figure 5:** Representation of the factors associated with shear stress.

$$\tau = \frac{\Delta P * r}{2L} \quad 65$$

Where  $\Delta P$  = pressure drop along pipe,  $R$  = radius of pipe,  $L$  = length of pipe, and  $r$  = distance from the center of the pipe.

The value of shear stress becomes a maximum when the distance from the center of the tube,  $r$ , is equal to the tube radius,  $R$  [16, 25]. Therefore, the maximum shear stress is located at the wall of the tube and is calculated using Equation 66.

$$\tau_{\max} = \tau_{\text{wall}} = \frac{\Delta P * R}{2L}$$

66

If the pressure drop across any section of tubing is known along with the radius and the length of the tube, the wall shear stress can be estimated.

### Effects of High Shear Stress Levels on Flowing Blood

Numerous researchers have investigated the importance of shear stress when looking at the flow of blood through tubes. It has been shown that high levels of shear can activate platelets and leukocytes as well as result in the destruction of red blood cells. Wall shear stress values between 1,500 and 3,000 dynes/cm<sup>2</sup> have been shown to cause measurable amounts of hemolysis [26, 27]. Leukocyte activation has been shown to occur at wall shear stress levels between 75 to 800 dynes/cm<sup>2</sup> [27]. Finally, platelets have been shown to be activated by wall shear stress levels between 60 and 100 dynes/cm<sup>2</sup> [9, 10, 27]. All of these factors can impair hemostasis as well as contribute to the post-operative morbidity associated with cardiopulmonary bypass.

The effect of vacuum assisted venous return on the formed elements of blood is not the focus of this study, but shear levels will be examined. The intention is that if there is significant increases in the levels of shear stress associated with VAVR, the study should be taken to the next level. The focus would be to compare activated platelet and complement levels as well as the level of hemolysis associated with VAVR.

### Cavitation

Cavitation is a phenomenon that occurs when gas is pulled out of solution to form gaseous emboli [16, 18]. The degree to which this occurs depends on the vapor pressure

of the liquid, the gas partial pressures, the pressure applied to the fluid, and the number of nucleation sites (which are necessary to form the gaseous emboli) [16, 18, 28].

Blood, with its hemoglobin content, has the ability to transport a significant quantity of dissolved oxygen and carbon dioxide. For this model, the blood conditions of interest are those of venous blood because that is the type of blood which will be subjected to the effects of VAVR. Common values for the partial pressures of venous blood are as follows [29, 30]:

$P_{O_2}$	40 mmHg
$P_{CO_2}$	46 mmHg
$P_{H_2O} @ 37^\circ C$	47 mmHg
$P_{N_2}$	571 mmHg
$P_{total}$	704 mmHg

When the pressure that the blood is being exposed to falls below the sum of the vapor pressure of water and partial pressures of the dissolved gases, gaseous micro-emboli can form. The likelihood or degree of cavitation to occur in a fluid is measured by the Thoma coefficient,  $K$  [16, 28]:

$$K = \frac{P_\infty - P_i}{\rho V^2 / 2} \quad 67$$

Where  $P_\infty$  = absolute static pressure,  $P_i$  = bubble pressure =  $P_{vapor} + P_{gas}$ ,  $\rho$  = liquid density, and  $V$  = reference velocity.

As mentioned previously, red blood cells, because of their gas content, are particularly susceptible to cavitation. The red blood cell can only withstand slight decreases in pressure [16, 31]. Also, blood to air interfaces are known to adversely effect



the formed elements of the blood resulting in an augmentation of the inflammatory response [7, 8, 9, 10].

Gaseous micro-emboli too small to be removed from the cardiopulmonary bypass circuit through filters or purge lines may also be transmitted to the patient resulting in stroke. Several studies have shown that assisted venous return exacerbates micro-emboli transmission into the arterial line of the cardiopulmonary bypass circuit. This is a potential source of stroke [4, 32].

The ability for cavitation to occur depends on the presence of nucleation sites in the blood [16, 28]. The critical pressure ( $P_c$ ) at which cavitation will occur depends on the initial radius of the bubble nucleus ( $R_0$ ) and the surface tension ( $\sigma$ ). The definition of the critical pressure is given in Equation 68 [16, 31].

$$P_c = P_v + P_g - \frac{2\sigma}{R_0} \quad 68$$

Where  $P_v$  = vapor pressure,  $P_g$  = gas pressure,  $R_0$  = initial radius of bubble, and  $\sigma$  = surface tension.

Because the bubble nucleus radius and the surface tension coefficient are difficult values to estimate, the critical pressure for cavitation will not be directly calculated [16, 31].

## **Laboratory Procedure**

The purpose of the laboratory was to verify the accuracy of the model proposed in this work for the two venous cannulation techniques utilizing vacuum assisted venous return. The circuit configuration was similar to those used by other researchers to study the flows through venous cannula(s) [6, 33, 34]. Due to the acceptance of this circuit configuration by other researchers who were studying similar parameters, the configuration was deemed acceptable for the purpose of this laboratory investigation.

Cannula sizes [in French where 3 mm = 1 French (Fr.)] were chosen from those manufacturers suggest while using VAVR and in a manner that would give a good representation of a small, medium, and large size cannula(s).

The type of experiment performed is classified as a *repeated measures* test [35]. The design of a *repeated measures* test is to use the same test subject for each of the independent variables. This allows for the controlling of inter-subject differences because the subject, the blood, is its own perfectly matched control [35].

To fulfill the criteria for a *repeated measures* test, the test circuit was primed with a mixture of blood and Plasmalyte solution similar to what would be used for cardiopulmonary bypass (CPB). This value can range from the 20% to 27%. For this investigation, a hematocrit of 22% was chosen to be the target value. The assumption is that this is a fair representation of what may be seen while on CPB and would result in a representative blood viscosity. The same blood was then exposed to each cannula included in the study as well as each level of applied vacuum. The independent variables were the cannula size and the amount of vacuum applied.

One caution in performing a *repeated measures* test on blood for any length of time would be the viability of the blood over the course of the test. Hemolysis levels may become significant and the effect on viscosity may become a confounding variable. For this reason, samples were drawn periodically during the investigation for a plasma free hemoglobin test. This is a commonly accepted measure of hemolysis and was therefore used to assess the condition of the blood being used.

Another concern with utilizing a repeated measures test design is the possibility of sequential or time dependent effects. If, in this study, the applied vacuum levels were incrementally administered, any time dependent effects of the circuit itself may confound the results by erroneously affecting the measured variables. For this reason, random numbers were applied to each level of vacuum to be applied to the system and for each trial to be performed. The goal was to evenly distribute any time dependent effect over all levels [35].

## Equipment

The following equipment was used in the laboratory investigation:

Bio-Medicus Centrifugal Pump. model: 550, s/n: 7194  
Medela Low Vacuum Aspirator. model: Basic 036, s/n: 971377  
IRMA SL Blood Analysis System. p/n: 443900, s/n: 21615  
Hatteland Instrumenting Ultrasonic Microbubble Detector. model: CMD10, s/n: 100  
Biotek Universal Pressure Meter. model: DPM-2 Plus, s/n: 141025  
DLP Pressure Display. model: 60000 Series, s/n: 418098  
Bard CPS Heat Exchanger. p/n: H-9430, lot #: 43BGX501-9602  
Heater/Cooler.  
Bovine Blood  
Avecor Cardiotomy/Venous Reservoir with Filter. model: CVR with Filter,  
lot #'s: HV00599, HV00625  
Terumo Hard Shell Venous Reservoir. model: CX\*SX10R, lot #'s: 990224, 990715H  
C-Clamp  
Avecor Soft Shell Venous Reservoir.  
Assorted 3/8" and 1/4" I.D. PVC tubing  
Assorted connectors and with and without luer locks

The following venous cannula were tested in the experiment:

### Single-Stage

1. DLP 24 Fr., model 66124
2. DLP 18 Fr., model 66118
3. DLP 12 Fr., model 66112

### Dual-Stage

1. DLP 29/29 Fr., model 91329
2. Sarns 28/38 Fr., model 4864

The circuit configurations used in this study are shown in Figures 6 & 7 on the following pages. The appropriate dimensions follow in Tables 1 & 2.

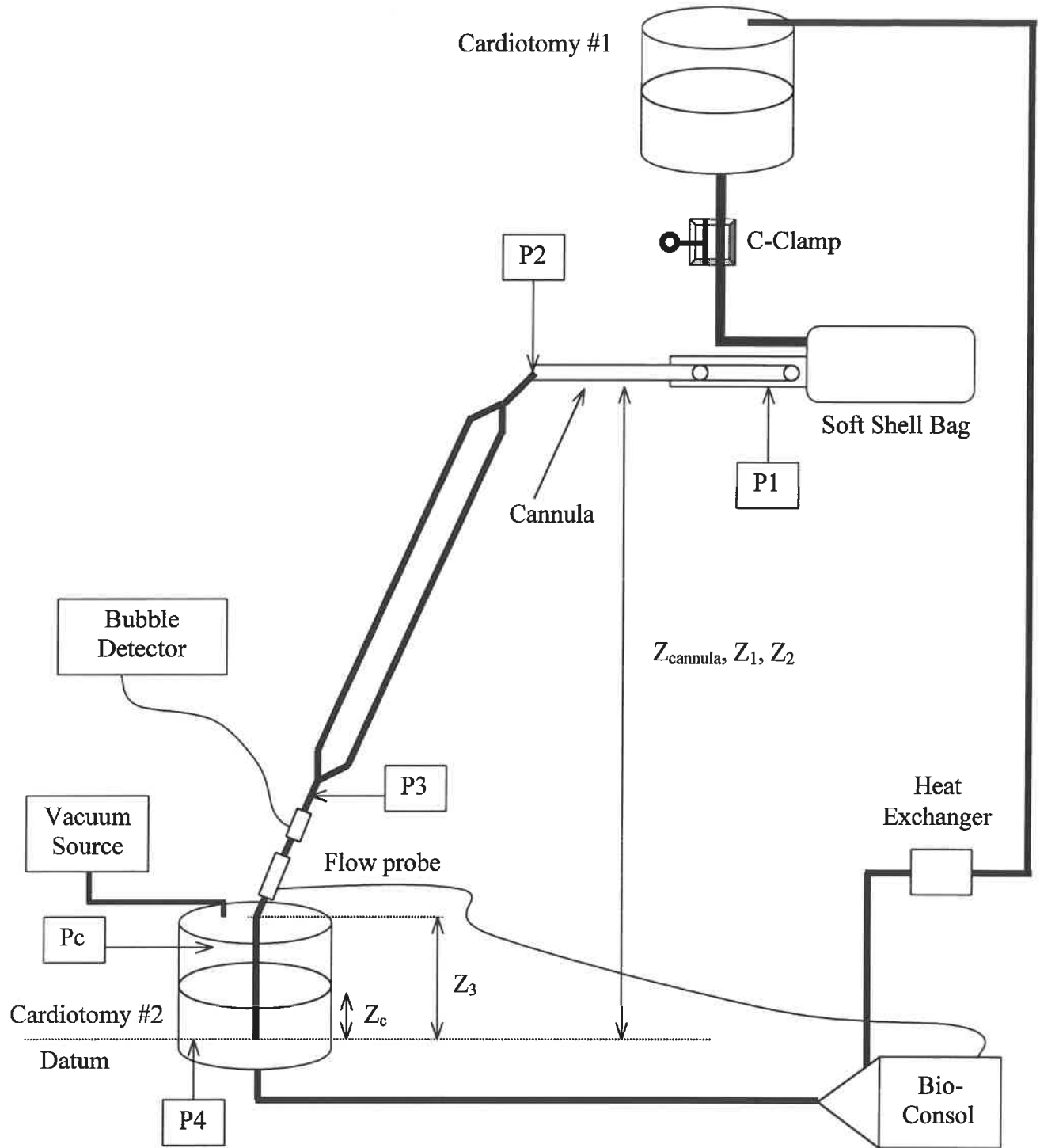


**Figure 6:** Circuit configuration used to test the model for the dual-stage venous cannula.

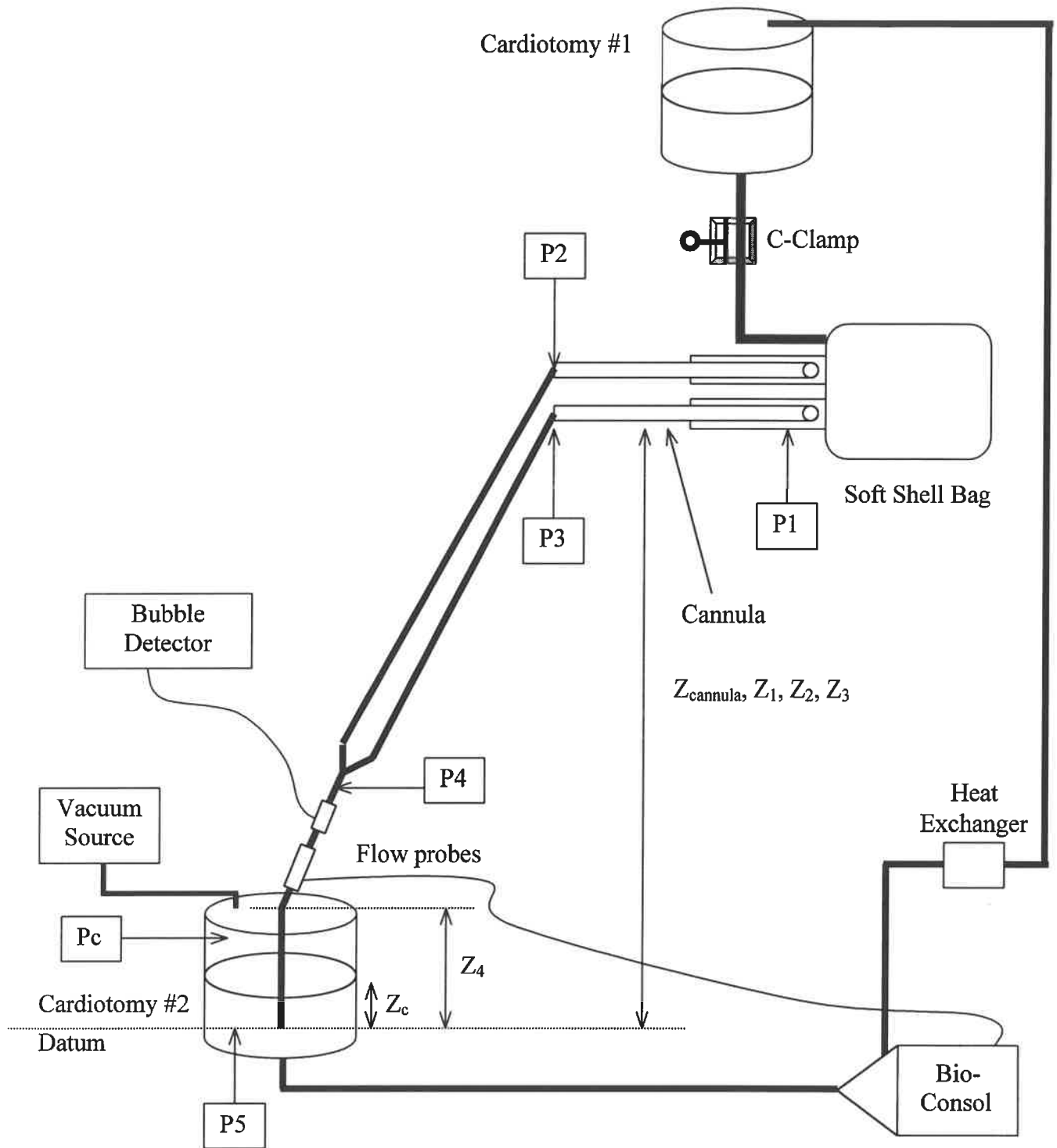


**Figure 7:** Circuit configuration used to test the model for the two single-stage venous cannula.

Parameter	Inner Diameter (cm)	Length (cm)
DLP 29/29 Fr. 91329	0.85	38.3
Sarns 32/40 Fr. 16472	0.95	39.1
Sarns 28/38 Fr. 4864	0.95	40.2
Length 2-4	0.95	153.7
Length 3-4	0.95	153.7
Length 4-5	0.95	76.7
Height $Z_{\text{cannula}}$ , $Z_1$ , $Z_2$	N/A	66.0
Height $Z_3$	N/A	38.1
Height $Z_C$	N/A	16.8

**Table 1:** Measured dimensions for the dual-stage cannula circuit of Figure 6.

Parameter	Inner Diameter (cm)	Length (cm)
DLP 24 Fr. 66124	0.60	34.3
DLP 18 Fr. 66118	0.45	34.0
DLP 12 Fr. 66112	0.25	30.5
Length 2-3	0.95	153.7
Length 3-4	0.95	153.7
Length 4-5	0.95	76.7
Height $Z_{\text{cannula}}$ , $Z_1$ , $Z_2$ , $Z_3$	N/A	66.0
Height $Z_4$	N/A	38.1
Height $Z_C$	N/A	16.8

**Table 2:** Measured dimensions for the single-stage cannula circuit of Figure 7.

The source of blood for this experiment was from a bovine specimen obtained from Ember Foods, Milwaukee, Wisconsin. Once the blood was collected it was heparinized with 40,000 units of beef lung heparin. It was then transported to the lab where it was filtered to remove any debris and bagged in Viaflex bags for storage. A sample was taken with a 3cc syringe and the IRMA blood gas analyzer was used to determine the hematocrit of the blood.

A second sample was also drawn for an activated clotting time (ACT). This was done periodically throughout the experiment and additional heparin was added, as needed, to maintain an ACT greater than 600 seconds.

With the circuit primed with the appropriate amount of blood and Plasmalyte and thoroughly de-aired, a second blood gas sample was drawn to verify the hematocrit using the IRMA blood gas analyzer. Also, a blood sample was drawn for plasma free hemoglobin measurement, this value was considered the baseline. The results of the blood gas data are located in Appendix A. The Hatteland Instrumentering CMD-20 Bubble Detector was also set up per the User's Manual with the counting interval set to 1 minute.

The pump speed (in RPMs) of the Bio-Medicus was initially set to a value that allowed the system to be at equilibrium. This meant that the fluid level in each reservoir remained constant. The circuit was inspected to verify that there was no air remaining on connectors or tubing walls.

Using the random number table generated by Quattro Pro, the pressure values to be used in the lab were assigned an order of application for each trial. The results of these random assignments are located in Appendix B. Using this table, the first cardiotomy pressure was applied to the circuit. Once the circuit flow was stabilized the pressure and flow readings were taken as depicted in the circuit diagrams. The results for the dual-stage cannulas are located in Appendix C and the results of the single-stage cannulas are located in Appendix D. Next, the bubble detector was activated for the one-minute count interval. The bubble counts for the dual-stage and the single-stage cannulas are located in Appendix E.

For each cannula, five trials were performed at each cardiotomy pressure. One sample of blood was taken for plasma free hemoglobin measurement and another for a blood



gas analysis after the completion of all five trials for any given cannula. At this point, the blood flow was stopped temporarily while the next cannula was connected into the circuit. The circuit was then restarted and the test procedure was repeated. This was done for each cannula included in the study.

## Results

Tables 3 and 4 give the flows obtained from the model as predicted by Equations 36, 60, and 61 along with the corresponding average measured flow. Detailed data from the model is available in Appendix F. The measured values of pressure and flow for each cannula are located in Appendices C and D.

Cardiotomy Pressure [mmHg]	28/38 Fr. Dual-Stage Cannula		29/29 Fr. Dual-Stage Cannula	
	Predicted Flow [L/min]	Average Measured Flow [L/min]	Predicted Flow [L/min]	Average Measured Flow [L/min]
0	3.43	$3.43 \pm 0.02$	3.33	$3.07 \pm 0.03$
-10	3.96	$4.05 \pm 0.11$	3.62	$3.61 \pm 0.05$
-20	4.44	$4.53 \pm 0.08$	4.05	$4.08 \pm 0.03$
-30	4.88	$4.94 \pm 0.03$	4.45	$4.50 \pm 0.06$
-40	5.30	$5.29 \pm 0.17$	4.83	$4.91 \pm 0.06$
-50	5.69	$5.70 \pm 0.02$	5.18	$5.31 \pm 0.03$
-60	6.05	$5.95 \pm 0.06$	5.51	$5.61 \pm 0.03$
-70	6.41	$6.32 \pm 0.07$	5.83	$5.85 \pm 0.03$
-80	6.74	$6.58 \pm 0.05$	6.13	$6.16 \pm 0.03$

**Table 3:** Predicted and average measured flows for each dual-stage cannula. Average measured flows reported as mean  $\pm$  standard deviation (n=5).

Cardiotomy Pressure [mmHg]	24 Fr. Single-Stage Cannula		18 Fr. Single-Stage Cannula		12 Fr. Single-Stage Cannula	
	Predicted Flow [L/min]	Average Measured Flow [L/min]	Predicted Flow [L/min]	Average Measured Flow [L/min]	Predicted Flow [L/min]	Average Measured Flow [L/min]
0	3.22	3.08 ± 0.03	2.37	2.22 ± 0.01	0.58	0.67 ± 0.01
-10	3.69	3.55 ± 0.05	2.73	2.60 ± 0.04	0.73	0.79 ± 0.01
-20	4.11	4.04 ± 0.05	3.06	2.96 ± 0.01	0.88	0.89 ± 0.01
-30	4.49	4.48 ± 0.04	3.26	3.30 ± 0.04	1.03	1.04 ± 0.01
-40	4.85	4.89 ± 0.04	3.52	3.67 ± 0.06	1.18	1.13 ± 0.01
-50	5.19	5.30 ± 0.02	3.77	3.94 ± 0.02	1.32	1.25 ± 0.02
-60	5.52	5.64 ± 0.05	4.01	4.26 ± 0.01	1.47	1.37 ± 0.01
-70	5.82	6.01 ± 0.08	4.24	4.50 ± 0.06	1.61	1.46 ± 0.01
-80	6.12	6.35 ± 0.06	4.46	4.76 ± 0.02	1.75	1.57 ± 0.01

**Table 4:** Predicted and average measured flows for each single-stage cannula. Average measured flows reported as mean ± standard deviation (n=5).

The graphs located in Figures 8 through 12 show the relationship between the predicted flows and the average measured flows of Tables 3 and 4 along with the corresponding error bars.

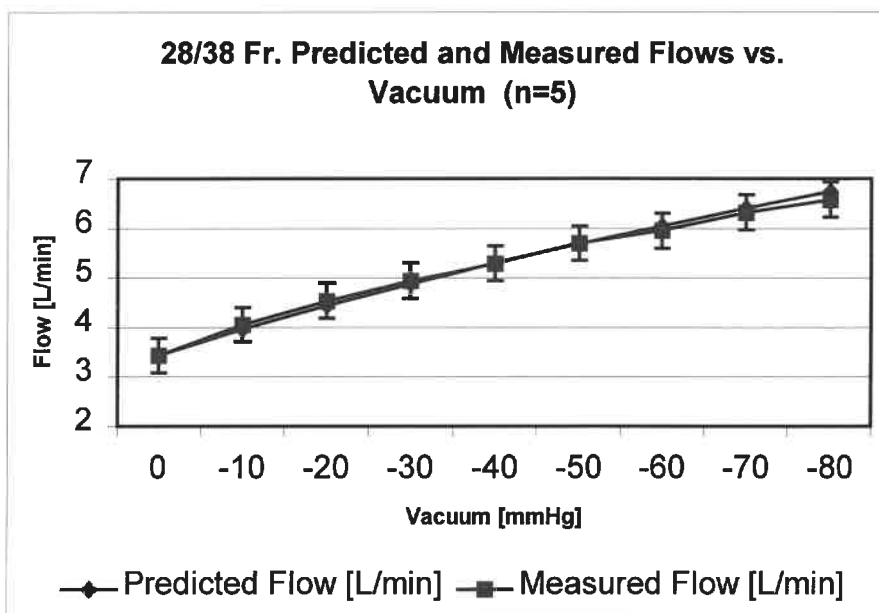


**Figure 8:** Graph of the predicted and average measured flows at each level of vacuum for the 28/38 Fr. dual-stage cannula

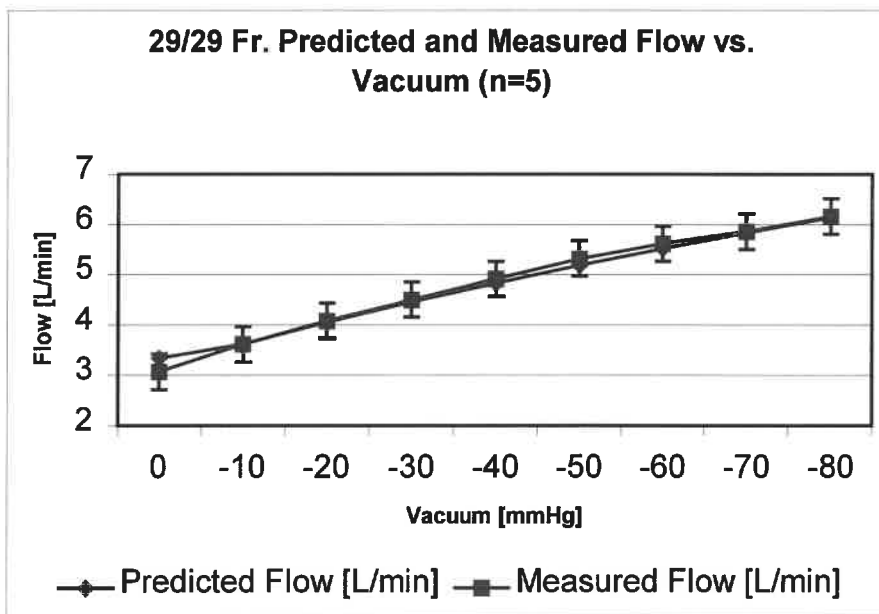


**Figure 9:** Graph of the predicted and average measured flows at each level of vacuum for the 29/29 Fr. dual-stage cannula.

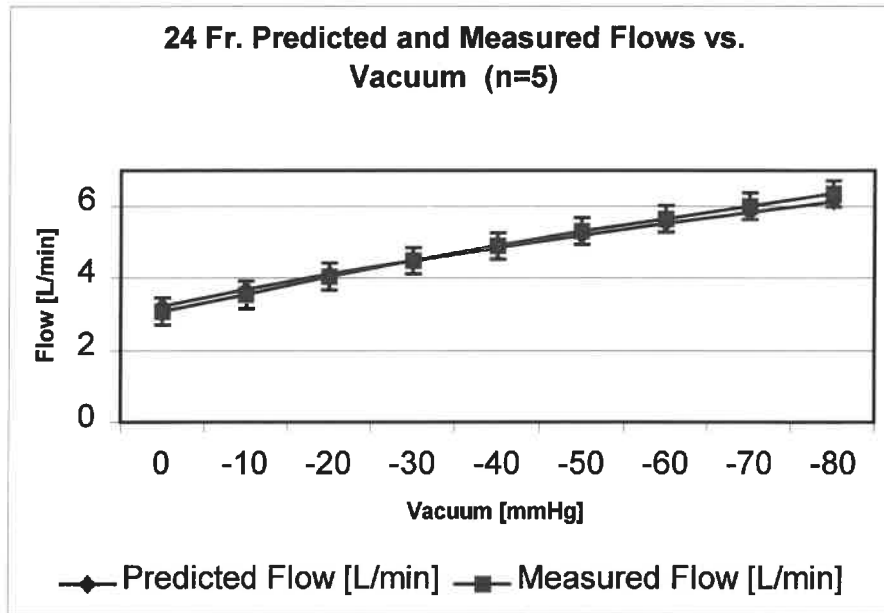


**Figure 10:** Graph of the predicted and average measured flows at each level of vacuum for the dual 24 Fr. single-stage cannulas.

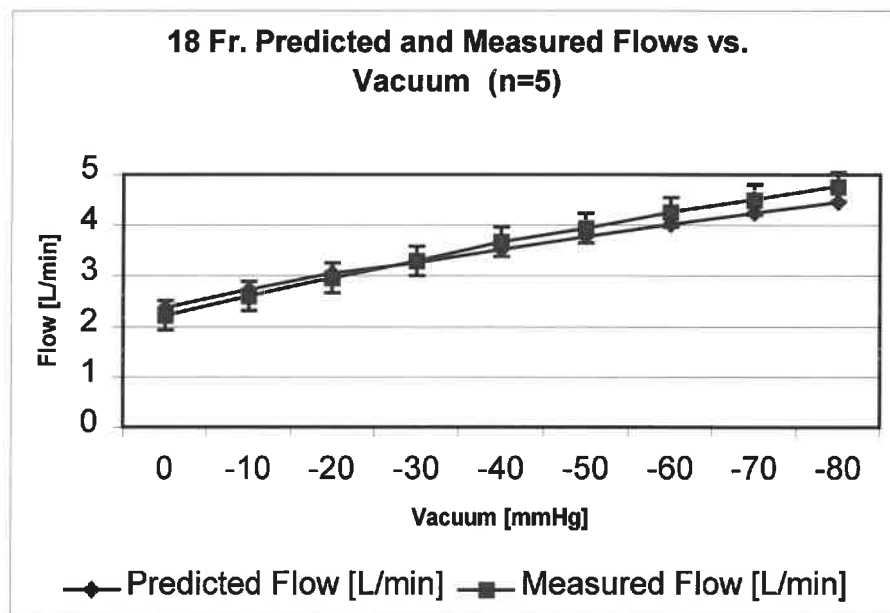


**Figure 11:** Graph of the predicted and average measured flows at each level of vacuum for the dual 18 Fr. single-stage cannulas.

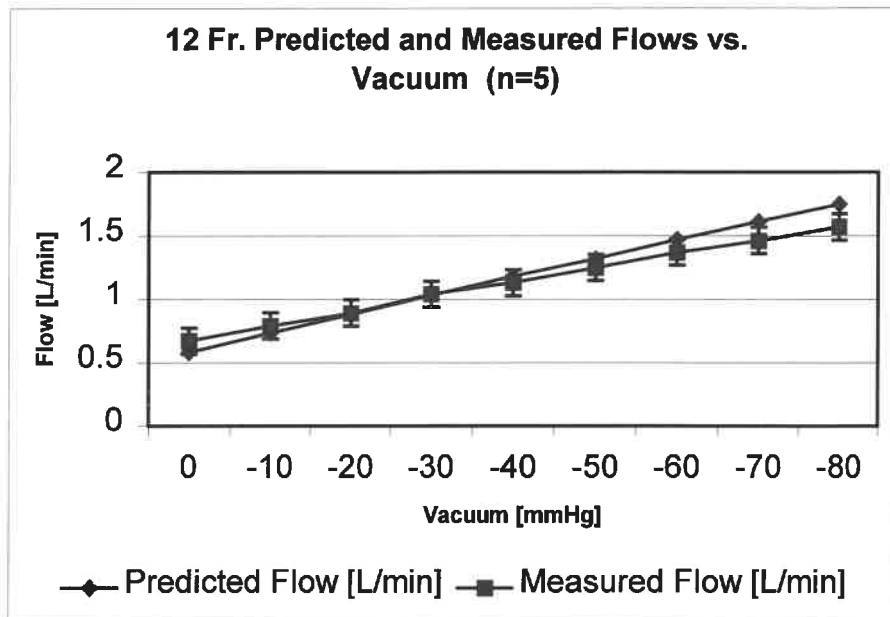


**Figure 12:** Graph of the predicted and average measured flows at each level of vacuum for the dual 12 Fr. single-stage cannulas.

Tables 5 and 6 give the predicted pressure drop values obtained from the combinations of Equations 36 & 37, Equations 60 & 62, and Equations 61 & 62 along with the average measured values for the pressure drop across each cannula.

Cardiotomy Pressure [mmHg]	28/38 Fr. Dual-Stage Cannula		29/29 Fr. Dual-Stage Cannula	
	Predicted Pressure Drop [mmHg]	Average Measured Pressure Drop [mmHg]	Predicted Pressure Drop [mmHg]	Average Measured Pressure Drop [mmHg]
0	19	12 ± 0.55	24	17 ± 0.55
-10	25	15 ± 1.10	28	20 ± 0.00
-20	31	17 ± 2.51	35	24 ± 0.55
-30	37	22 ± 0.55	42	28 ± 0.00
-40	43	22 ± 5.86	49	32 ± 0.45
-50	50	28 ± 0.55	57	36 ± 0.55
-60	56	30 ± 0.84	64	40 ± 1.64
-70	63	32 ± 1.64	71	43 ± 0.84
-80	69	34 ± 1.14	78	46 ± 0.55

**Table 5:** Predicted and average measured pressure drop for each dual-stage cannula. Average measured pressure drop reported as mean ± standard deviation (n=5).

Cardiotomy Pressure [mmHg]	24 Fr. Single-Stage Cannula		18 Fr. Single-Stage Cannula		12 Fr. Single-Stage Cannula	
	Predicted Pressure Drop [mmHg]	Average Measured Pressure Drop [mmHg]	Predicted Pressure Drop [mmHg]	Average Measured Pressure Drop [mmHg]	Predicted Pressure Drop [mmHg]	Average Measured Pressure Drop [mmHg]
0	23	14 ± 0.55	30	21 ± 0.55	36	31 ± 0.55
-10	30	18 ± 0.84	39	27 ± 0.84	45	38 ± 0.55
-20	37	22 ± 0.45	48	32 ± 0.89	55	46 ± 0.45
-30	44	26 ± 0.84	53	38 ± 0.45	64	55 ± 0.84
-40	51	29 ± 0.00	61	43 ± 0.55	74	62 ± 0.45
-50	58	34 ± 0.45	70	50 ± 0.84	83	70 ± 0.89
-60	65	38 ± 0.45	78	56 ± 0.45	93	78 ± 0.55
-70	72	41 ± 0.89	86	62 ± 1.00	105	87 ± 0.89
-80	79	45 ± 0.84	94	68 ± 0.55	112	96 ± 0.84

**Table 6:** Predicted and average measured pressure drop for each single-stage cannula. Average measured pressure drop reported as mean ± standard deviation (n=5).



The graphs located in Figures 13 through 17 show the relationship between the predicted and the average measured pressure drop across each cannula along with the corresponding error bars.

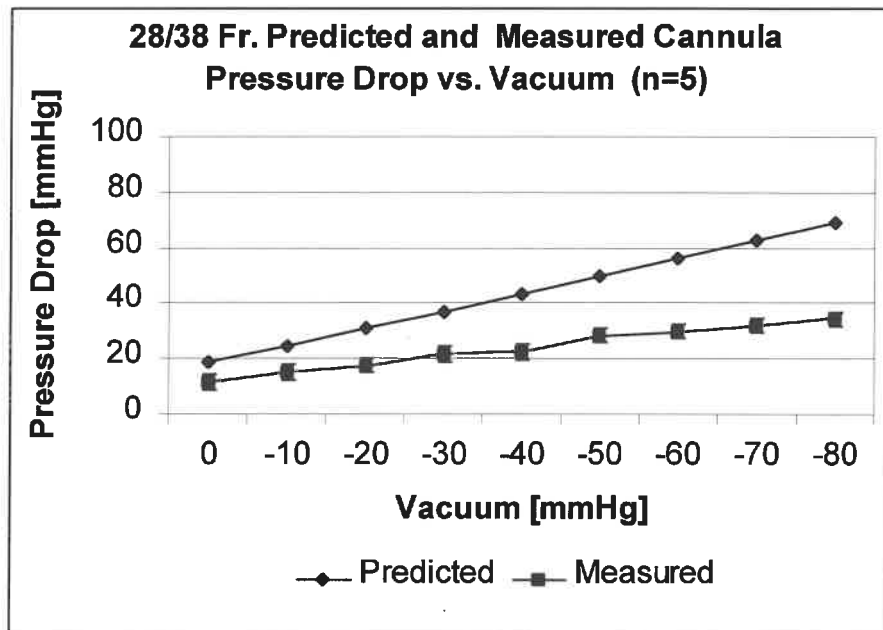


**Figure 13:** Graph of the predicted and average measured pressure drop at each level of vacuum for the 28/38 Fr. dual-stage cannula.

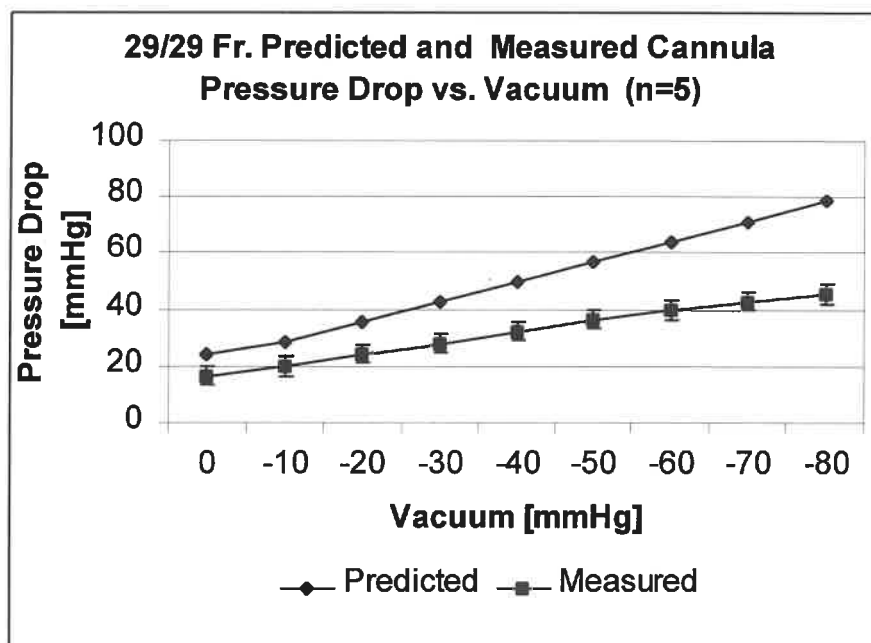


**Figure 14:** Graph of the predicted and average measured pressure drop at each level of vacuum for the 29/29 Fr. dual-stage cannula.

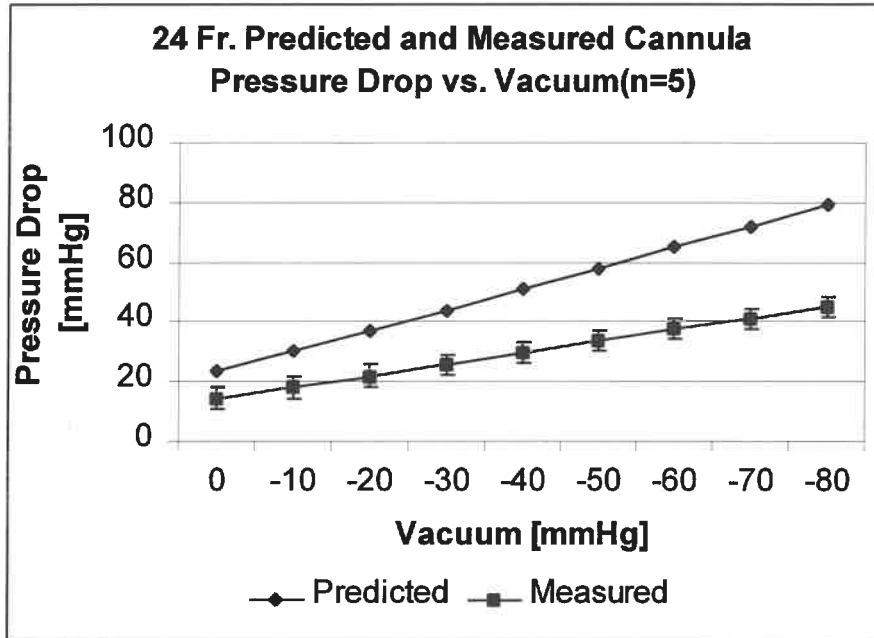


**Figure 15:** Graph of the predicted and average measured pressure drop at each level of vacuum for the 24 Fr. single-stage cannula.

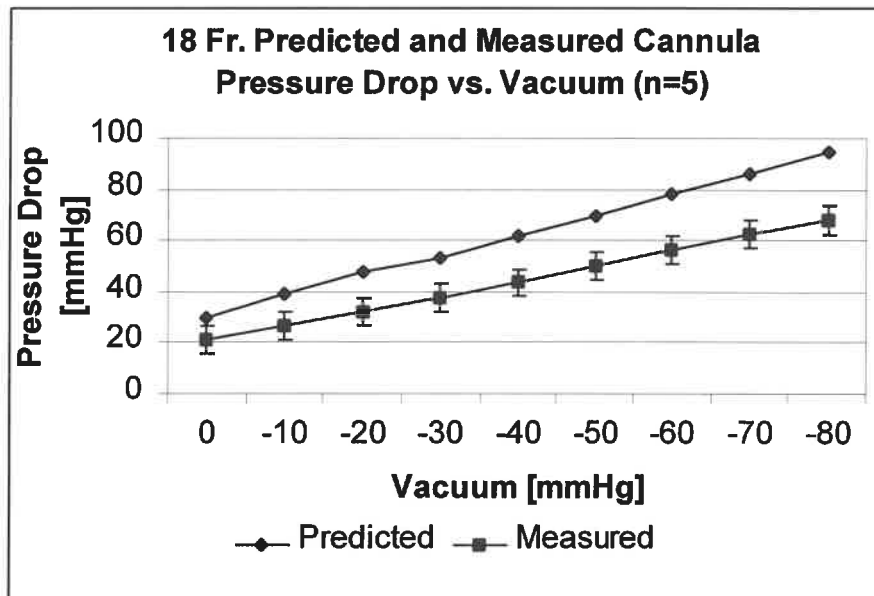


**Figure 16:** Graph of the predicted and average measured pressure drop at each level of vacuum for the 18 Fr. single-stage cannula.

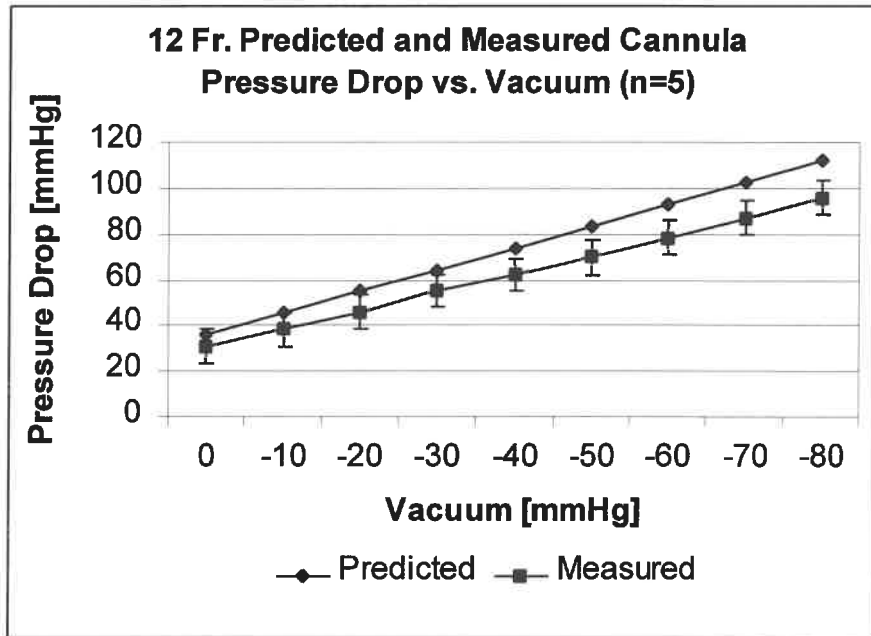


**Figure 17:** Graph of the predicted and average measured pressure drop at each level of vacuum for the 12 Fr. single-stage cannula.

Tables 7 and 8 give the predicted cannula wall shear stress values using the cannula pressure drop data of Tables 5 and 6 in combination with Equation 66 and the estimated average wall shear stress values for each cannula.

Cardiotomy Pressure [mmHg]	28/38 Fr. Dual-Stage Cannula		29/29 Fr. Dual-Stage Cannula	
	Predicted Wall Shear Stress [dynes/cm <sup>2</sup> ]	Average Estimated Wall Shear Stress [dynes/cm <sup>2</sup> ]	Predicted Wall Shear Stress [dynes/cm <sup>2</sup> ]	Average Estimated Wall Shear Stress [dynes/cm <sup>2</sup> ]
0	147	91 ± 4.31	179	123 ± 4.05
-10	194	120 ± 8.63	210	148 ± 6.19
-20	243	137 ± 19.77	261	180 ± 12.15
-30	292	170 ± 4.31	313	207 ± 4.05
-40	341	176 ± 46.12	365	238 ± 3.31
-50	392	224 ± 4.31	418	269 ± 0.00
-60	443	235 ± 6.59	472	294 ± 4.05
-70	494	250 ± 12.94	526	317 ± 0.00
-80	546	271 ± 8.98	580	337 ± 4.05

**Table 7:** Predicted and average estimated values of wall shear stress for each dual-stage cannula. Average estimated wall shear stress reported as mean ± standard deviation (n=5).

Cardiotomy Pressure [mmHg]	24 Fr. Single-Stage Cannula		18 Fr. Single-Stage Cannula		12 Fr. Single-Stage Cannula	
	Predicted Wall Shear Stress [dynes/cm <sup>2</sup> ]	Average Estimated Wall Shear Stress [dynes/cm <sup>2</sup> ]	Predicted Wall Shear Stress [dynes/cm <sup>2</sup> ]	Average Estimated Wall Shear Stress [dynes/cm <sup>2</sup> ]	Predicted Wall Shear Stress [dynes/cm <sup>2</sup> ]	Average Estimated Wall Shear Stress [dynes/cm <sup>2</sup> ]
0	136	91 ± 3.19	132	123 ± 2.42	98	84 ± 1.50
-10	176	120 ± 4.88	171	148 ± 3.69	124	104 ± 1.50
-20	216	137 ± 2.61	210	180 ± 3.94	150	125 ± 1.22
-30	256	170 ± 4.88	234	207 ± 1.97	176	151 ± 2.29
-40	297	176 ± 0.00	271	238 ± 2.42	202	170 ± 1.22
-50	338	224 ± 2.61	307	269 ± 3.69	228	191 ± 2.44
-60	379	235 ± 2.61	343	294 ± 1.97	254	213 ± 1.50
-70	420	250 ± 5.21	379	317 ± 4.41	280	238 ± 2.44
-80	461	271 ± 4.88	416	337 ± 2.42	306	262 ± 2.29

**Table 8:** Predicted and average estimated values of wall shear stress for each single-stage cannula. Average estimated wall shear stress reported as mean ± standard deviation (n=5).

The graphs located in Figures 18 through 22 show the relationship between the predicted and the average estimated value of wall shear stress across each cannula along with the corresponding error bars.

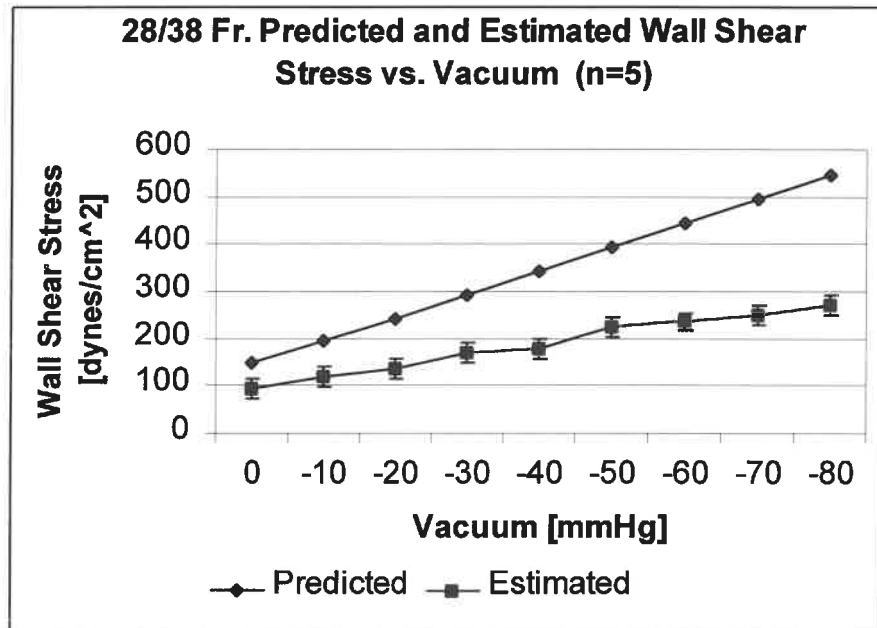


**Figure 18:** Graph of the predicted and average estimated wall shear stress values for the 28/38 Fr. dual-stage cannula.

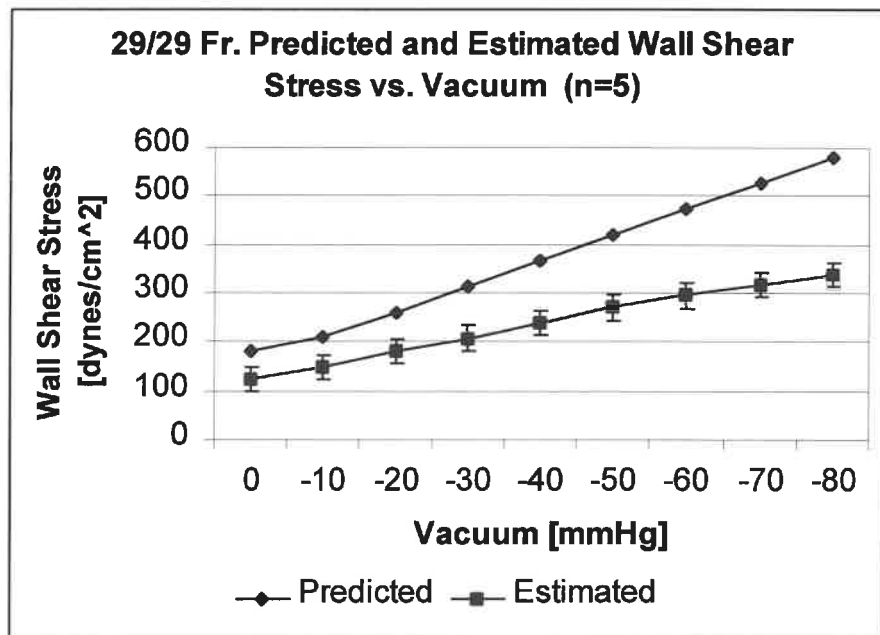


**Figure 19:** Graph of the predicted and average estimated wall shear stress values for the 29/29 Fr. dual-stage cannula.

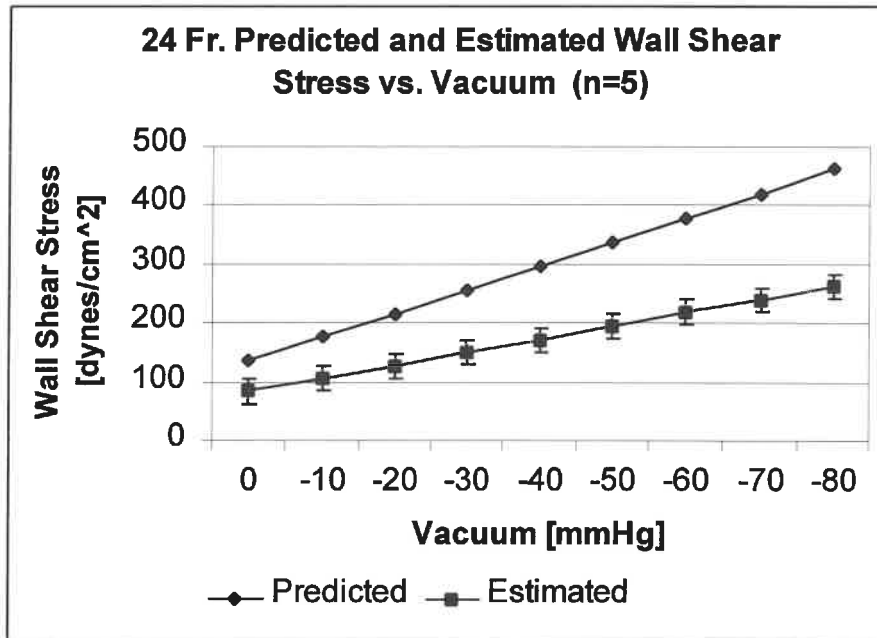


**Figure 20:** Graph of the predicted and average estimated wall shear stress values for the 24 Fr. single-stage cannula.

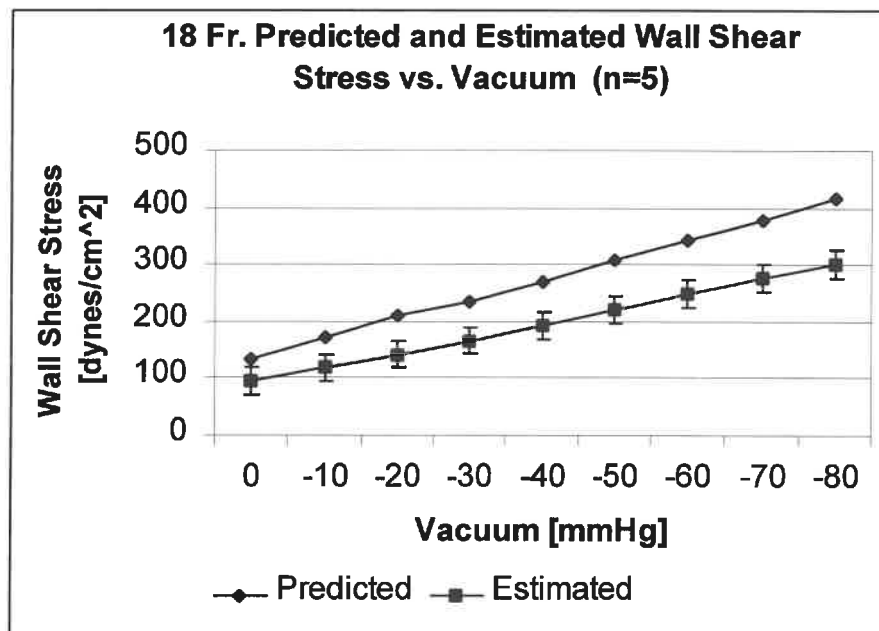


**Figure 21:** Graph of the predicted and average estimated wall shear stress values for the 18 Fr. single-stage cannula.

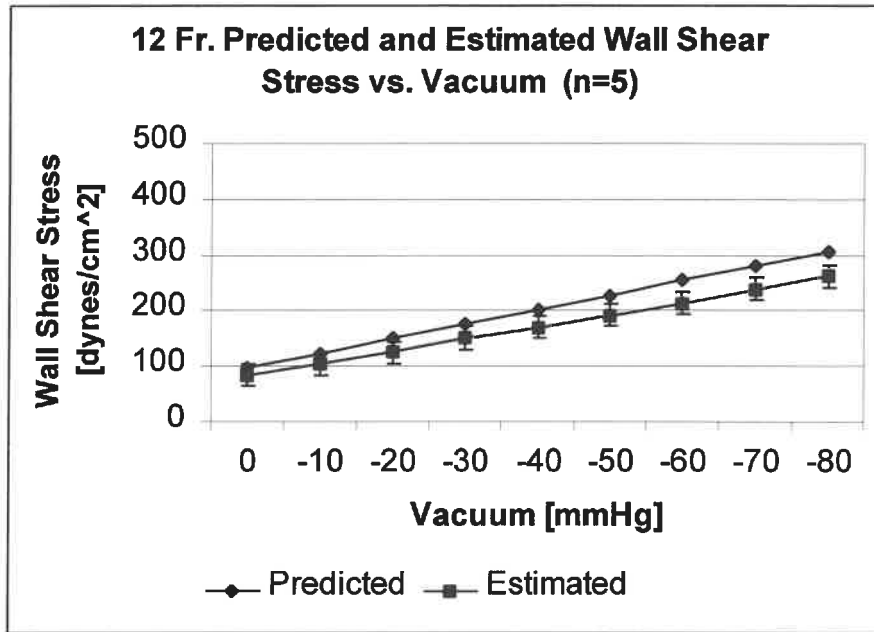


**Figure 22:** Graph of the predicted and average estimated wall shear stress values for the 12 Fr. single-stage cannula.



Tables 9 through 13 give the average bubble counts for each size level and at each level of vacuum. Level 1 denotes bubble sizes in the range of 0-10 microns, Level 2 denotes bubble sizes between 10-20 microns, Level 3 denotes bubble sizes between 20-30 microns, and Level 4 denotes bubbles sizes between 30-40 microns.

Cardiotomy Pressure [mmHg]	Average Bubble Count			
	Level 1	Level 2	Level 3	Level 4
0	23 ± 8.91	9 ± 4.97	136 ± 8.23	165 ± 9.32
-10	19 ± 5.27	11 ± 0.45	128 ± 4.21	156 ± 5.13
-20	13 ± 8.62	11 ± 0.55	128 ± 5.94	156 ± 6.91
-30	17 ± 7.05	11 ± 0.45	129 ± 3.78	158 ± 4.51
-40	13 ± 9.26	13 ± 5.37	127 ± 5.89	156 ± 3.94
-50	9 ± 9.07	11 ± 0.45	132 ± 3.13	161 ± 4.27
-60	14 ± 11.55	11 ± 0.71	131 ± 6.02	159 ± 7.14
-70	22 ± 0.71	11 ± 0.45	128 ± 4.66	156 ± 5.70
-80	12 ± 7.01	13 ± 5.61	125 ± 6.30	154 ± 9.04

**Table 9:** Average bubble counts at each level of vacuum for the 28/38 Fr. dual-stage cannula. Bubble counts reported as mean ± standard deviation (n=5).

Cardiotomy Pressure [mmHg]	Average Bubble Count			
	Level 1	Level 2	Level 3	Level 4
0	17 ± 8.50	10 ± 0.45	124 ± 2.59	151 ± 2.59
-10	14 ± 6.48	13 ± 5.27	125 ± 5.15	149 ± 7.09
-20	19 ± 5.32	11 ± 0.55	128 ± 5.63	156 ± 6.98
-30	9 ± 6.98	10 ± 0.84	122 ± 10.06	148 ± 11.97
-40	21 ± 1.23	10 ± 0.84	123 ± 6.30	150 ± 7.54
-50	14 ± 7.60	10 ± 0.00	121 ± 1.00	147 ± 1.41
-60	19 ± 5.50	10 ± 0.55	123 ± 6.40	150 ± 8.01
-70	22 ± 0.55	11 ± 0.55	126 ± 3.96	153 ± 4.39
-80	19 ± 4.97	10 ± 0.55	125 ± 5.26	153 ± 6.38

**Table 10:** Average bubble counts at each level of vacuum for the 29/29 Fr. dual-stage cannula. Bubble counts reported as mean ± standard deviation (n=5).

Cardiotomy Pressure [mmHg]	Average Bubble Count			
	Level 1	Level 2	Level 3	Level 4
0	20 ± 6.14	12 ± 1.30	147 ± 4.77	179 ± 5.36
-10	18 ± 6.26	12 ± 0.55	146 ± 2.49	178 ± 3.36
-20	17 ± 10.41	12 ± 0.55	145 ± 4.77	176 ± 5.36
-30	7 ± 6.96	15 ± 7.40	142 ± 2.05	175 ± 3.27
-40	10 ± 9.20	10 ± 1.79	146 ± 14.50	175 ± 12.14
-50	14 ± 7.92	12 ± 1.48	144 ± 5.64	175 ± 4.97
-60	16 ± 8.61	12 ± 6.10	142 ± 7.13	172 ± 16.24
-70	17 ± 7.68	10 ± 1.64	145 ± 18.04	176 ± 15.53
-80	12 ± 11.37	12 ± 6.31	141 ± 11.23	171 ± 6.42

**Table 11:** Average bubble counts at each level of vacuum for the 24 Fr. single-stage cannula. Bubble counts reported as mean ± standard deviation (n=5).

Cardiotomy Pressure [mmHg]	Average Bubble Count			
	Level 1	Level 2	Level 3	Level 4
0	10 ± 5.74	13 ± 0.58	155 ± 5.12	186 ± 6.29
-10	12 ± 11.80	12 ± 0.55	154 ± 5.17	186 ± 6.34
-20	13 ± 8.37	13 ± 1.30	158 ± 4.24	189 ± 8.77
-30	17 ± 14.14	13 ± 1.82	153 ± 9.99	185 ± 12.27
-40	16 ± 13.24	13 ± 0.89	159 ± 7.99	199 ± 11.63
-50	9 ± 8.64	14 ± 0.71	150 ± 10.73	192 ± 11.42
-60	10 ± 4.51	14 ± 1.00	157 ± 2.39	195 ± 3.13
-70	13 ± 11.37	14 ± 2.17	154 ± 1.10	188 ± 7.30
-80	13 ± 4.76	13 ± 0.45	156 ± 8.35	189 ± 8.62

**Table 12:** Average bubble counts at each level of vacuum for the 18 Fr. single-stage cannula. Bubble counts reported as mean ± standard deviation (n=5).

Cardiotomy Pressure [mmHg]	Average Bubble Count			
	Level 1	Level 2	Level 3	Level 4
0	10 ± 10.31	13 ± 0.55	158 ± 6.35	192 ± 7.50
-10	7 ± 7.09	13 ± 0.55	159 ± 4.16	190 ± 5.03
-20	19 ± 11.11	14 ± 5.41	158 ± 9.13	192 ± 11.19
-30	19 ± 11.22	13 ± 0.45	161 ± 10.41	194 ± 6.42
-40	13 ± 10.29	12 ± 5.37	151 ± 2.30	176 ± 5.48
-50	19 ± 10.83	14 ± 0.55	156 ± 6.89	195 ± 8.11
-60	19 ± 13.07	11 ± 1.14	152 ± 9.76	181 ± 12.44
-70	24 ± 11.73	14 ± 5.50	144 ± 8.08	186 ± 10.21
-80	15 ± 12.34	14 ± 0.84	151 ± 6.28	193 ± 8.04

**Table 13:** Average bubble counts at each level of vacuum for the 12 Fr. single-stage cannula. Bubble counts reported as mean ± standard deviation (n=5).

The graphs located in Figures 23 through 27 show the relationship between vacuum and bubble counts at each size level for each cannula.

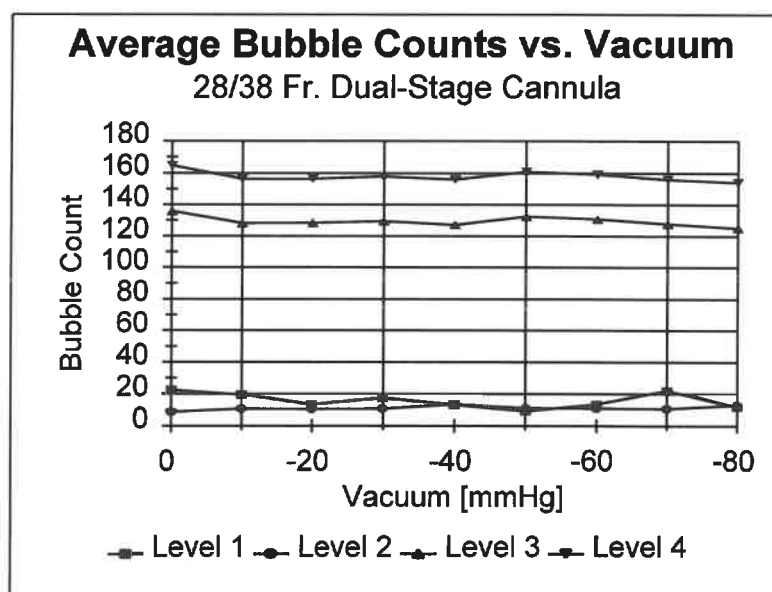


**Figure 23:** Graph of the average bubble count per level versus the amount of vacuum applied for the 28/38 Fr. dual-stage cannula.

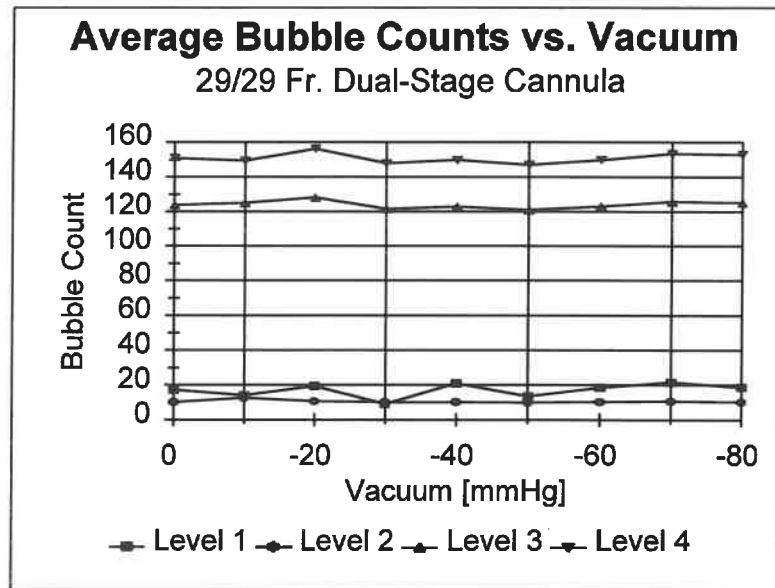


**Figure 24:** Graph of the average bubble count per level versus the amount of vacuum applied for the 29/29 Fr. dual-stage cannula.

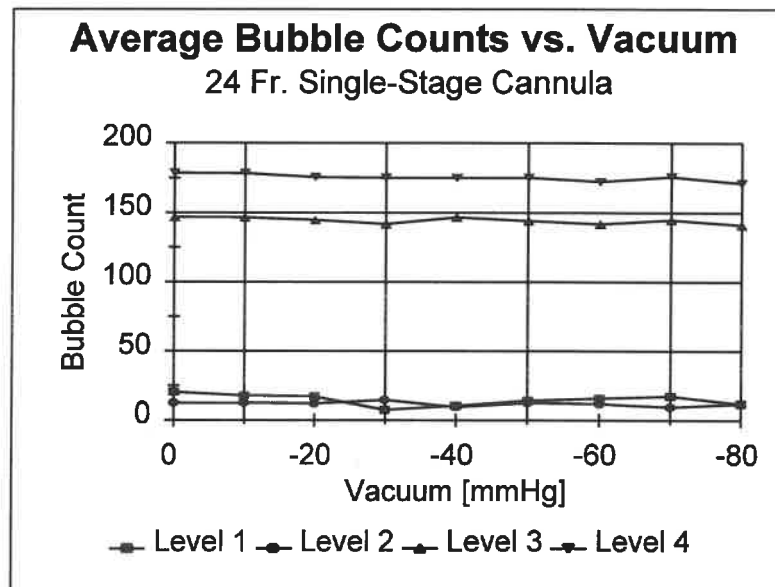


**Figure 25:** Graph of the average bubble count per level versus the amount of vacuum applied for the 24 Fr. single-stage cannula.

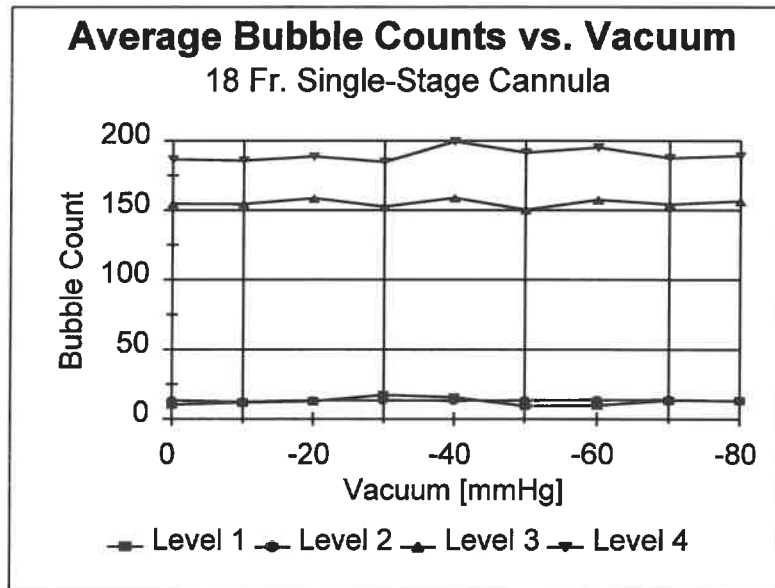


**Figure 26:** Graph of the average bubble count per level versus the amount of vacuum applied for the 18 Fr. single-stage cannula.

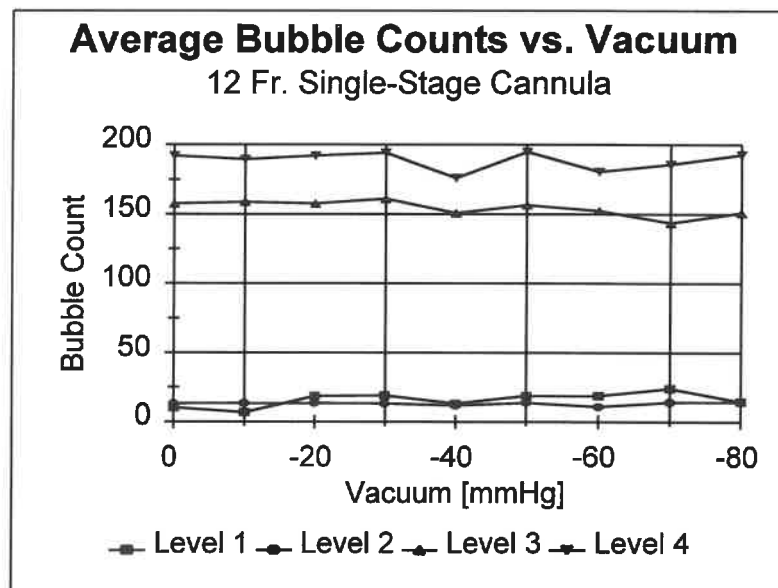


**Figure 27:** Graph of the average bubble count per level versus the amount of vacuum applied for the 12 Fr. single-stage cannula.

As mentioned on page 9, due to the unique geometry of the cannula tips (inlets), values of the inlet head loss constant,  $K_L$ , for each cannula would need to be determined from experimental data. These values could then be used in the model for the calculation of the head loss due to the entrance into the cannula.

In order to determine the inlet head loss constant for each cannula, the measured flows were entered into the model of Appendix F. The *Solve for* function of Quattro Pro was then used to determine the inlet head loss constant for each level of vacuum assuming a right atrial pressure,  $P_1$ , of zero. The average value of  $K_L$  for each cannula was then used as the constant in the model. Table 14 gives the average value of  $K_L$  for each cannula.

Cannula	Inlet Head Loss Constant, $K_L$
28/38 Fr. Dual-Stage Cannula	5.96
29/29 Fr. Dual-Stage Cannula	4.36
24 Fr. Single-Stage Cannula	4.39
18 Fr. Single-Stage Cannula	1.33
12 Fr. Single-Stage Cannula	0.18

**Table 14:** Average value of the inlet head loss constant for each cannula.

### Analysis

To compare the predicted and measured flow values, linear regression was performed on the combined data. The measured flows were the dependent variable and the predicted flows were the independent variable. The resulting regression equation (Equation 69) applies to all five cannulas tested over the range of vacuum specified.

$$\text{measured flow} = 0.00565 + (0.9977 * \text{predicted flow}) \quad 69$$

Figure 28 shows the plot of all the measured flow values for each cannula versus the predicted flow values along with the regression line of Equation 69.

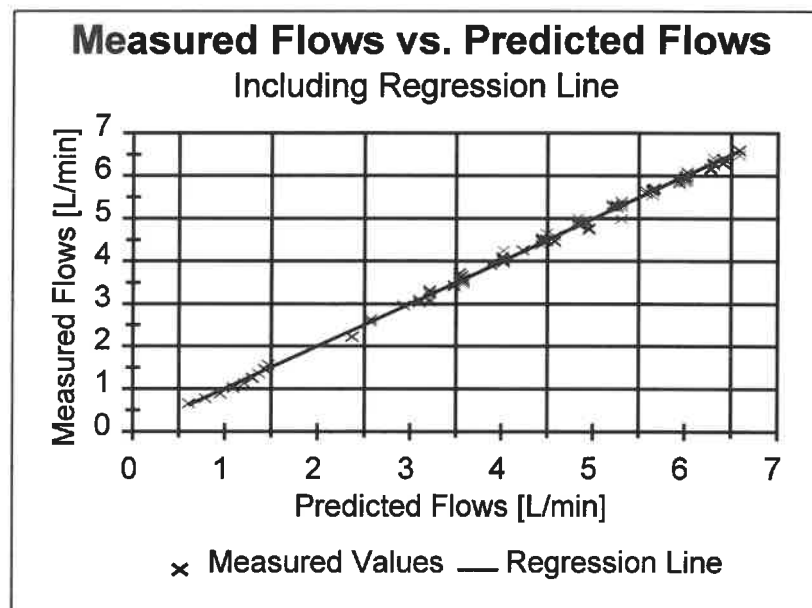


**Figure 28:** Graph of the measured versus predicted flows for all cannulas tested along with the corresponding regression line.

To verify the model's ability to accurately predict flow rates, the slope (bold) of Equation 69 was tested using the t-statistic equation shown in Equation 70 [38].

$$t = \frac{b - \beta_0}{s_b} \quad 70$$

Where  $b$  is the slope being tested,  $\beta_0$  is the slope value that  $b$  is being compared with, and  $s_b$  is an estimate of the variance from the regression data. If the model results matched the measured data exactly, the slope of the regression line would be 1.0 [35]. Therefore, by substituting the slope of Equation 69 in for  $b$  and substituting 1.0 in for  $\beta_0$ , a t-statistic was calculated. The value of the t-statistic comparing the slope of Equation 69 to 1.0 was  $-0.722$  (Appendix H). With a t-critical value of 1.645 for an alpha ( $\alpha$ ) of 0.05 and 224 degrees of freedom, it was concluded that the model is an exact predictor of flow over the range of vacuum specified.

The next step was to perform a two-way ANOVA test to see if there was any significant difference between the flows at each level of vacuum and between each cannula. The ANOVA analysis showed a statistically significant difference between the flows when compared to vacuum levels and between cannula ( $p = 0.00$ ). The Bonferroni t-test was then used to determine between which levels of vacuum was a significant change in flow detected. The results showed that for each increased level of vacuum applied (-10 mmHg increments) there was a statistically significant increase in flow ( $p < 0.05$ ).



The next set of data analyzed was the predicted and estimated values of cannula wall shear stress. As was done in the comparison of predicted to measured flows, linear regression was performed. The regression equation is shown in Equation 71.

$$\text{estimated wall shear stress} = 36.390 + (0.5569 * \text{predicted wall shear stress}) \quad 71$$

Figure 29 shows the plot of all the estimated wall shear stress values for each cannula versus the predicted values along with the regression line from Equation 71.

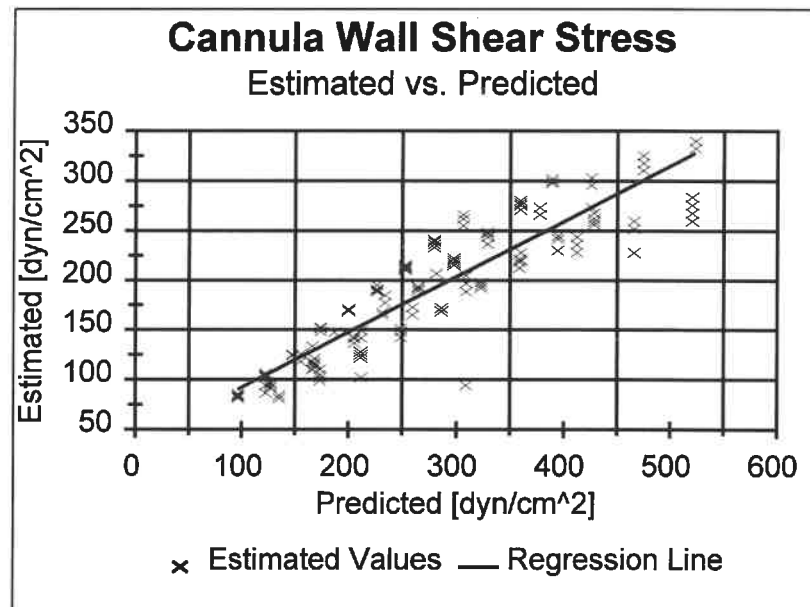


**Figure 29:** Graph of the estimated versus predicted cannula wall shear stress values for all cannulas tested along with the corresponding regression line.

The slope of Equation 71 was compared to 1.0 using Equation 70. The t-statistic was calculated to be -17.013 (Appendix H). Comparing this to a critical t-value of 1.645 with an alpha of 0.05 and 224 degrees of freedom, it was concluded that there was a statistically significant difference between the predicted and measured values. Therefore,

the model is not an exact predictor of cannula wall shear stress over the range of vacuum tested.

If the model was not predictive of cannula wall shear stress, the slope of the regression equation would be zero meaning no relationship between the estimated and predicted values exists. Equation 70 was again used but with  $\beta_0$  set to zero to test this. The calculated t-statistic was 21.38 (Appendix H). Comparing this to the critical t-value equal to 1.645, it was concluded with a  $\alpha$  equal to 0.05 and 224 degrees of freedom, that there was a statistically significant difference between the slope of the shear stress regression line and zero. Therefore, it was concluded that the model is predictive of cannula wall shear stress values over the range of vacuum specified.

Next, a two-way ANOVA test was performed to see if there was any significant difference between the wall shear stress values at each level of vacuum and between each cannula. The ANOVA analysis showed a statistically significant difference between the wall shear stress values when compared to vacuum levels and between each cannula ( $p = 0.00$ ). The Bonferroni t-test was then used to determine between which levels of vacuum was a significant change detected. The results showed that for each level of vacuum applied (-10 mmHg increments), there was a statistically significant increase in the estimated wall shear stress for each cannula ( $p < 0.05$ ).

The last set of data to be analyzed was the bubble counts for each cannula at each level of vacuum. Using a one-way ANOVA test it was shown that there were significant differences in the bubble counts when compared to vacuum levels for the 28/38 Fr. ( $p = 0.05$ ) and 29/29 Fr. ( $p = 0.004$ ) dual-stage cannulas as well as the 12 Fr. ( $p = 0.02$ ) single-stage cannula. The Bonferroni t-Test showed that the increases in bubble counts

did not correlate with the increased levels of vacuum. Therefore, it can be concluded that increasing the level of vacuum applied to the cardiectomy over the range of 0 to -80 mmHg did not result in an increase in the number of gaseous microemboli detected.

### **Conclusions**

From the statistical analysis performed on the data collected in the laboratory investigation and that obtained from the model, it can be concluded that the model is an exact predictor of flow over the range of vacuum specified. This was evidenced by the calculated t-statistic that verified that the slope of Equation 69 was not significantly different from 1.0.

The model was not an accurate predictor of wall shear stress for the cannulas and vacuum pressures used in this work. This was evidenced by the calculated t-statistic that showed the slope of Equation 71 was significantly different from 1.0. However, it was shown that the model was predictive of the wall shear stress by the t-statistic that verified the slope of Equation 71 was significantly different from 0.0.

A potential source for the discrepancy between the predicted and the measured values could be the assumptions made in the development of the model. One possible source of error is the assumption that Reynolds numbers of 2300 or greater represent turbulent flow. In this model, Reynolds numbers greater than or equal to 2300 resulted in the use of a different equation for the friction factor used in determining the frictional head loss as shown in Equation 11. This equation accounts for the added resistance that results from turbulent flow. The added resistance corresponds to an increased pressure drop. In reality, the transition from laminar to turbulent flow is not easily predicted. There are conditions where laminar flow will tend to stay laminar and turbulent flow will

tend to stay turbulent, regardless of the Reynolds number. But, because the frictional head loss calculation in this model depends strictly on the Reynolds number, the result may be the overestimation of the pressure drop, and hence the estimated wall shear stress, using Equation 66.

The analysis of the bubble count data indicates that cavitation was not an issue with respect to vacuum assisted venous return. But, by performing power analysis (see Appendix G) on the bubble count data, it can be shown that there is a strong chance that the conclusions drawn from the bubble count analysis are not accurate (strong probability of a Type II error). Therefore, the potential for cavitation with the use of VAVR should not be ignored for several reasons. First, the data collected in this work had too low of a power to make any reasonable determinations about the effect that VAVR can have on cavitation. Second, there have been reports of increased amounts of micro-air detected in the arterial line while using VAVR [4,32]. Third, as the amount of vacuum is increased, the likelihood of pulling gas out of blood increases as shown by the Thoma coefficient equation on page 24 (Equation 67).

In order to determine the effects of VAVR on cavitation, a study focused on this phenomenon needs to be performed with more data collected. One particular point of interest would be pump inlets, especially centrifugal pumps, which are known to generate high levels of negative pressure. Focusing on the effect VAVR has on the pump inlet pressure and the cavitation potential would be worthwhile.

Even though the model did not accurately predict wall shear stress values, both the model and the lab results show that the use of VAVR significantly increases cannula wall shear stress. This should be a major focus for follow-up studies. As mentioned on page

2, numerous studies have shown the detrimental effects of shear stress on platelets, complement, and red blood cells. The magnitude of the increase in wall shear stress shown in this work warrants further investigation on this topic as it pertains to the use of VAVR. The next logic step would be to collect data on platelet and activated complement levels (C3a and C5a in particular) from *in vivo* animal experiments.

The model proposed in this paper could be a useful tool for the perfusionist who chooses to utilize the technique of VAVR. It can also be beneficial to other researchers who are investigating the effects of vacuum assisted venous return.

## References

1. Jegger D, Tevæarai HT, Horisberger J, Mueller XM, Boone Y, Pierrel N, Seigneul I, von Segesser LK. Augmented venous return for minimally invasive open heart surgery with selective caval cannulation. *European Journal of Cardio-thoracic Surgery* 1999;16:312-316.
2. Darling E, Kaemmer D, Lawson S, Smigla G, Collins K, Shearer I, Jagers J. Experimental use of an ultra-low prime neonatal cardiopulmonary bypass circuit utilizing vacuum-assisted venous drainage. *Journal of Extracorporeal Technology* 1998;30(4):184-189.
3. Lau CL, Posther KE, Stephenson GR, Lodge A, Lawson JH, Darling EM, Davis RD, Ungerleider RM, Jagers J. Mini-circuit cardiopulmonary bypass with vacuum assisted venous drainage: feasibility of an asanguineous prime in the neonate. *Perfusion* 1999;14:389-396.
4. Willcox T, Mitchell S, Gorman D. Venous air in the bypass circuit: a source of arterial line emboli exacerbated by vacuum-assisted venous drainage. *Annals of Thoracic Surgery* 1999;68:1285-1289.
5. Taketani S, Sawa Y, Masai T, Ichikawa H, Kagisaki K, Yamaguchi T, Ohtake S, Matsuda H. A novel technique for cardiopulmonary bypass using vacuum system for venous drainage with pressure relief valve: an experimental study. *Artificial Organs* 1998;22(4):337-341.
6. Kurusz M, Deyo D, Sholar A, Tao W, Zwischenberger J. Laboratory testing of femoral venous cannulae: effect of size, position and negative pressure on flow. *Perfusion* 1999;14:379-387.
7. Gu YJ, Boonstra PW, Graaff R, Rijnsburger AA, Mungroop H, van Oeveren W. Pressure drop, shear stress, and activation of leukocytes during cardiopulmonary bypass: a comparison between hollow fiber and flat sheet membrane oxygenators. *Artificial Organs* 2000, 24(1):43-48.
8. Kao WJ, Sapatnekar S, Hiltner A, Anderson J. Complement-mediated leukocyte adhesion on poly (etherurethane ureas) under shear stress in vitro. *Journal of Biomedical Materials Research* 1996;32:99-109.
9. Kroll M, Hellums JD, McIntire LV, Schafer AI, Moake JL. Platelets and shear stress. *Blood* 1996;88(5):1525-1541.
10. Weiss DJ, Evanson OA, McClenahan D, Fagliari J, Walcheck. Shear-induced platelet activation and platelet-neutrophil aggregate formation by equine platelets. *Am J Vet Res* 1998;59(10):1243-1246.

11. Miller BE, Levy JH. The inflammatory response to cardiopulmonary bypass. *Journal of Cardiothoracic and Vascular Anesthesia* 1997;11(3):355-366.
12. Utley JR. The history of the concept of inflammatory responses to cardiopulmonary bypass. *Perfusion* 1996;11:190-195.
13. Vennard, John K. *Elementary Fluid Mechanics, 4th Edition*. John Wiley & Sons, Inc., New York. Copyright © 1961.
14. Benedict, Robert P. *Fundamentals of Pipe Flow*. John Wiley & Sons, Inc., New York. Copyright © 1980.
15. Harris, Norman C., Edwin M. Hemmerling and A. James Mallman. *Physics Principles and Applications, Fifth Edition*. McGraw-Hill, Inc., New York. Copyright © 1990.
16. Yang, Wen-Jei. *Biothermal-Fluid Sciences Principles and Applications*. Hemisphere Publishing Corporation, New York. Copyright © 1989.
17. Jeppson, Roland W. *Analysis of Flow in Pipe Networks*. Ann Arbor Science, Ann Arbor, Michigan. Copyright © 1976.
18. Cheremisinoff, Nicholas P. *Fluid Flow Pumps, Pipes and Channels*. Ann Arbor Science, Ann Arbor Michigan. Copyright © 1981.
19. Hoppensteadt, Frank C. and Charles S. Peskin. *Mathematics in Medicine and the Life Sciences*. Springer-Verlag New York, Inc., New York. Copyright © 1992.
20. Mead, Daniel W. *Hydraulic Machinery*. McGraw-Hill Book Company, Inc., New York. Copyright © 1933.
21. McClain, Clifford H. *Fluid Flow in Pipes, Second Edition*. The Industrial Press, New York. Copyright © 1963.
22. Bennett, C. O. and J. E. Meyers. *Momentum, Heat, and Mass Transfer, Third Edition*. McGraw-Hill, Inc., New York. Copyright © 1982.
23. Fung, Y.C. *Biomechanics Circulation, Second Edition*. Springer-Verlag New York, Inc., New York. Copyright © 1997.
24. Govier, G.W. and K. Aziz. *The Flow of Complex Mixtures in Pipes*. Robert E. Krieger Publishing Company, Huntington, New York. Copyright © 1977.
25. Fournier, Ronald L. *Basic Transport Phenomena in Biomedical Engineering*. Taylor & Francis, Philadelphia, Pennsylvania. Copyright © 1999.

26. Wirz, H. J. and J. J. Smolderen. *Numerical Methods in Fluid Dynamics*. McGraw-Hill, Inc., New York. Copyright © 1978.
27. Gross, David R. and Ned H.C. Hwang. *The Rheology of Blood, Blood Vessels and Associated Tissues*. Sijthoff & Noordhoff, Rockville, Maryland. Copyright © 1981.
28. Davies, Robert. *Cavitation in Real Liquids*. Elsevier Publishing Company, New York. Copyright © 1964.
29. Berne, Robert M. and Matthew N. Levy. *Physiology, Third Edition*. Mosby Year Book, Inc., St. Louis, Missouri. Copyright © 1993.
30. Guyton, Arthur C. and John E. Hall. *Textbook of Medical Physiology, Ninth Edition*. W.B. Saunders Company, Philadelphia, Pennsylvania. Copyright © 1996.
31. Tomich, Angela. In Vitro Quantitative Analysis of Air Production with Varying Base Flows. Library of the Milwaukee School of Engineering. AC805.T66 1998.
32. Rider S, Simon L, Rice B, Poulton C. Assisted venous drainage, venous air, and gaseous microemboli transmission into the arterial line: an in-vitro study. *Journal of Extracorporeal Technology* 1998;30(4):160-165.
33. Kugai T, Koja K, Kusaba A. An in-vitro evaluation of venous cannula in a simulated partial (femoro-femoral) cardiopulmonary bypass circuit. *Artificial Organs* 1995;19(2):154-160.
34. Wenger R, Bavaria J, Ratcliffe M, Bogen D, Edmunds LH. Flow dynamics of peripheral venous catheters during extracorporeal membrane oxygenation with a centrifugal pump. *Journal of Thoracic Cardiovascular Surgery* 1988;96:478-484.
35. Portney, Leslie G. and Mary P. Watkins. *Foundations of Clinical Research Applications to Practice*. Appleton & Lange, Norwalk, Connecticut. Copyright © 1993.
36. Hensley, Frederick A., Jr. and Donald E. Martin. *A Practical Approach to Cardiac Anesthesia, Second Edition*. Little, Brown and Company, Boston, Massachusetts. Copyright © 1995.
37. Brodie, John E. and Ronald B. Johnson. *The Manual of Clinical Perfusion, Second Edition*. Glendale Medical Corporation, Augusta, Georgia. Copyright © 1997.
38. Daniel, Wayne W. *Biostatistics: A Foundation for Analysis in the Health Sciences, Fifth Edition*. John Wiley & Sons, Inc., New York, New York. Copyright © 1991.



**Appendix A:**  
**Blood Gas Data**

Blood Gas Values

Cannula	Part #	Size [Fr.]	pO <sub>2</sub> [mmHg]	pCO <sub>2</sub> [mmHg]	pN <sub>2</sub> [mmHg]	pH <sub>2</sub> O <sub>2</sub> [mmHg]	pTotal [mmHg]	K <sup>+</sup> [mMoles]	Hct	Initial (I)/Final (F)	PFHGB [mg/dL]	ID #
Initial	-	-	24.2	66.3	571.0	47.0	708.5	6.42	30.6	-	-	-
Sams	16472	32/40	29.4	42.8	571.0	47.0	690.2	6.03	21.6	I	335.0	1A
Sams	16472	32/40	29.1	31.4	571.0	47.0	678.5	6.13	21.1	F	384.9	1B
Sams	4864	28/38	30.1	30.3	571.0	47.0	678.4	6.16	20.5	I	377.7	2A
Sams	4864	28/38	37.6	24.5	571.0	47.0	680.1	6.09	20.6	F	384.9	2B
DLP	91329	29/29	40.4	23.7	571.0	47.0	682.1	6.06	21.0	I	505.7	3A
DLP	91329	29/29	35.8	22.2	571.0	47.0	676.0	6.08	19.9	F	346.4	3B
DLP	66124	24	36.0	20.8	571.0	47.0	674.8	6.05	20.3	I	352.5	4A
DLP	66124	24	40.8	17.9	571.0	47.0	676.7	6.03	20.0	F	370.9	4B
DLP	66118	18	47.7	17.3	571.0	47.0	683.0	6.00	20.4	I	434.7	5A
DLP	66118	18	47.0	17.5	571.0	47.0	682.5	5.97	19.9	F	498.9	5B
DLP	66112	12	47.8	18.0	571.0	47.0	683.8	6.00	21.3	I	491.8	6A
DLP	66112	12	48.9	17.8	571.0	47.0	684.7	6.02	20.1	F	459.8	6B

Hematocrit

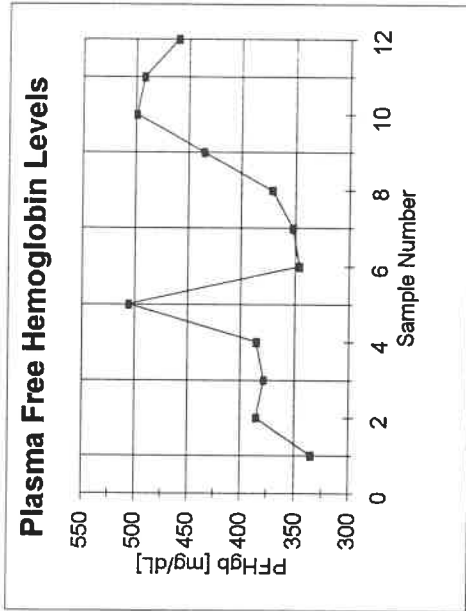
Mean	20.558
Standard Error	0.165
Median	20.450
Mode	19.900
Standard Deviation	0.573
Variance	0.328
Coefficient of Variation	2.79%
Portney pg 327-328	

Potassium

Mean	6.052
Standard Error	0.016
Median	6.040
Mode	6.000
Standard Deviation	0.056
Variance	0.003
Coefficient of Variation	0.92%

Plasma Free Hemoglobin

Mean	411.93
Standard Error	18.18
Median	384.90
Mode	384.90
Standard Deviation	62.96
Variance	3964.23
Coefficient of Variation	15.28%



#### Regression Output for Plasma Free Hemoglobin Data:

Constant	342.9788
Std Err of Y Est	52.45342
R Squared	0.369048
No. of Observations	12
Degrees of Freedom	10
X Coefficient(s)	10.60839
Std Err of Coef.	4.386376

#### Analysis of Variance: One Way

##### Summary

Groups	Count	Sum	Average	Variance
PFHgb	12	4943.2	411.9333	3964.232
Sample #	12	78	6.5	13

##### Analysis of Variance

##### Source of Variation

	SS	df	MS	F	P-value	F-crit
Between Groups	986257.1	1	986257.1	495.9516	1.4E-16	4.300949
Within Groups	43749.55	22	1988.616			
Total	1030007	23				

\*\*Bonferroni t-Test showed a significant difference between PFHgb levels between samples.

**Appendix B:**  
Random Number Tables

Trial #1		Trial #2		Trial #3		Trial #4		Trial #5	
Random #	Pressure	Random #	Pressure	Random #	Pressure	Random #	Pressure	Random #	Pressure
0.2982	0	0.9413	0	0.0625	0	0.1770	0	0.8268	0
0.7151	-10	0.6362	-10	0.1072	-10	0.2441	-10	0.4993	-10
0.0330	-20	0.3522	-20	0.6649	-20	0.7203	-20	0.2969	-20
0.8744	-30	0.0257	-30	0.2895	-30	0.6106	-30	0.7047	-30
0.5342	-40	0.9734	-40	0.6781	-40	0.8295	-40	0.8220	-40
0.6316	-50	0.7572	-50	0.3441	-50	0.0446	-50	0.0567	-50
0.8910	-60	0.7081	-60	0.1727	-60	0.4264	-60	0.4544	-60
0.2575	-70	0.9116	-70	0.7230	-70	0.4462	-70	0.1884	-70
0.9316	-80	0.0164	-80	0.9401	-80	0.0079	-80	0.9486	-80
0.2772	-90	0.1098	-90	0.9605	-90	0.4266	-90	0.6438	-90
0.7158	-100	0.0163	-100	0.5459	-100	0.1863	-100	0.3759	-100

Trial #	Order [Pressures in mmHg]										
	1st	2nd	3rd	4th	5th	6th	7th	8th	9th	10th	11th
1	-20	-70	-90	0	-40	-50	-10	-100	-30	-60	-80
2	-100	-80	-30	-90	-20	-10	-60	-50	-70	0	-40
3	0	-10	-60	-30	-50	-100	-20	-40	-70	-80	-90
4	-80	-50	0	-100	-10	-60	-90	-70	-30	-20	-40
5	-50	-70	-20	-100	-60	-10	-90	-30	-40	0	-80

**Appendix C:**  
Measured Flow and Cannula Pressure Drop Data for the Dual-  
Stage Cannulas

Pc [mmHg]	Flow [L/min]								
	0	-10	-20	-30	-40	-50	-60	-70	-80
Sarns 28/38 Fr. Dual- Stage Cannula	3.45	4.25	4.66	4.90	5.00	5.68	5.86	6.43	6.49
	3.43	4.00	4.50	4.98	5.35	5.69	5.91	6.30	6.61
	3.41	3.97	4.53	4.97	5.41	5.73	5.98	6.28	6.62
	3.44	4.02	4.47	4.92	5.40	5.70	5.97	6.32	6.59
	3.41	4.01	4.48	4.93	5.29	5.69	6.01	6.26	6.58
DLP 29/29 Fr. Dual- Stage Cannula	3.06	3.59	4.06	4.52	4.86	5.34	5.58	5.83	6.14
	3.05	3.65	4.10	4.56	4.94	5.30	5.59	5.88	6.18
	3.05	3.67	4.12	4.39	5.01	5.34	5.64	5.87	6.15
	3.11	3.56	4.06	4.51	4.88	5.29	5.59	5.82	6.14
	3.06	3.57	4.04	4.50	4.87	5.28	5.65	5.83	6.20

Pc [mmHg]	Pressure Drop Across Cannula [mmHg]								
	0	-10	-20	-30	-40	-50	-60	-70	-80
Sarns 28/38 Fr. Dual- Stage Cannula	12	17	13	21	12	28	29	29	34
	11	15	19	22	24	29	29	33	34
	12	15	19	22	26	28	30	32	36
	12	15	18	22	25	29	30	33	33
	11	14	18	21	25	28	31	32	35
DLP 29/29 Fr. Dual- Stage Cannula	16	20	24	28	32	36	40	42	45
	17	20	24	28	32	36	37	43	46
	17	20	25	28	33	37	41	43	46
	16	20	25	28	32	36	40	42	45
	17	20	24	28	32	37	41	44	46

**Appendix D:**  
Measured Flow and Cannula Pressure Drop Data for the Single-  
Stage Cannulas



Pc [mmHg]	Flow [L/min]								
	0	-10	-20	-30	-40	-50	-60	-70	-80
DLP 12 Fr. Single- Stage Venous Cannula	0.66	0.78	0.88	1.04	1.13	1.24	1.37	1.48	1.57
	0.67	0.78	0.9	1.05	1.13	1.28	1.37	1.45	1.58
	0.67	0.79	0.9	1.02	1.14	1.24	1.36	1.46	1.56
	0.66	0.79	0.89	1.03	1.14	1.26	1.37	1.47	1.58
	0.67	0.79	0.9	1.05	1.13	1.25	1.36	1.46	1.57
DLP 18 Fr. Single- Stage Venous Cannula	2.21	2.58	2.96	3.32	3.74	3.93	4.28	4.46	4.74
	2.21	2.57	2.95	3.24	3.61	3.96	4.26	4.60	4.76
	2.24	2.65	2.97	3.32	3.65	3.92	4.25	4.47	4.79
	2.22	2.63	2.95	3.28	3.62	3.95	4.25	4.49	4.75
	2.23	2.58	2.97	3.33	3.71	3.94	4.25	4.50	4.78
DLP 24 Fr. Single- Stage Venous Cannula	3.03	3.57	4.05	4.51	4.93	5.26	5.68	5.97	6.40
	3.11	3.54	4.04	4.45	4.84	5.32	5.56	6.10	6.43
	3.10	3.61	4.03	4.53	4.86	5.30	5.70	6.01	6.31
	3.09	3.53	4.05	4.47	4.87	5.31	5.65	6.07	6.33
	3.05	3.48	4.05	4.44	4.94	5.31	5.63	5.89	6.28

Pc [mmHg]	Pressure Drop Across Cannula [mmHg]								
	0	-10	-20	-30	-40	-50	-60	-70	-80
DLP 12 Fr. Single- Stage Venous Cannula	31	37	45	53	61	68	76	86	94
	30	37	45	55	61	70	77	84	95
	30	38	45	53	61	68	77	86	93
	31	38	44	54	61	69	76	86	93
	31	37	45	54	60	68	76	85	94
	32	38	47	56	63	70	81	90	98
	30	39	46	57	64	73	81	87	100
	31	40	46	56	64	71	77	90	94
	31	39	47	57	63	71	79	89	99
	30	39	47	57	64	72	80	88	98
DLP 18 Fr. Single- Stage Venous Cannula	22	26	30	37	43	49	55	60	66
	21	25	32	37	42	50	55	62	66
	21	27	32	37	43	48	55	60	67
	22	26	31	36	43	50	55	62	66
	21	27	32	37	42	49	54	61	67
	22	27	32	39	45	51	58	63	69
	21	26	33	38	44	50	58	65	69
	21	28	32	38	44	50	57	63	70
	21	26	33	39	44	51	57	64	70
	21	28	33	38	44	50	58	64	70
DLP 24 Fr. Single- Stage Venous Cannula	14	17	21	26	29	32	37	39	45
	15	18	22	24	29	33	36	41	44
	14	19	22	26	29	33	37	41	43
	15	18	22	25	29	33	37	41	44
	15	17	22	25	29	33	37	40	43
	14	18	21	26	30	34	39	40	47
	14	18	22	25	30	34	37	43	46
	14	19	21	26	30	35	39	42	45
	14	18	22	26	30	34	38	43	46
	14	17	22	26	29	34	38	39	46

**Appendix E:**  
Measured Bubble Counts for the Dual-Stage and Single-Stage  
Cannulas

**28/38 Fr. Dual-Stage Cannula:**

[illegible]

**29/29 Fr. Dual-Stage Cannula:**

[illegible]

### 24 Fr. Single-Stage Cannula:

[illegible]

### 18 Fr. Single-Stage Cannula:

[illegible]

### 12 Fr. Single-Stage Cannula:

[illegible]

**Appendix F:**  
Predicted Data from the Model for Each Cannula



$V_{DE}^{2/2g}$	$h_{in}$	$h_{out}$	$h_{i/A,B}$	$h_{i/C,D}$	$h_{i/D,E}$	$h_{diverg, flow}$	$h_{converg, flow}$	Cardiotomy Pressure mmHg	$P_1$ [mmHg]	$P_2$ [mmHg]	$P_3$ [mmHg]	$P_4$ [mmHg]	Pressure Drop 1 to 2 [mmHg]
3.300	14.55	3.30	6.18	6.29	11.57	0.45	0.63	0	-0.00	-18.71	-5.66	13.10	18.71
4.393	19.37	4.39	7.94	7.26	14.86	0.61	0.43	-10	0.00	-24.69	-12.46	3.10	24.69
5.521	24.34	5.52	9.69	8.14	18.14	0.76	0.23	-20	0.00	-30.80	-19.23	-6.90	30.80
6.675	29.43	6.68	11.44	8.95	21.42	0.92	0.01	-30	-0.00	-37.03	-26.00	-16.90	37.03
7.853	34.62	7.85	13.19	9.71	24.69	1.08	-0.20	-40	-0.00	-43.35	-32.76	-26.90	43.35
9.049	39.90	9.05	14.93	10.42	27.95	1.25	-0.42	-50	-0.00	-49.75	-39.52	-36.90	49.75
10.262	45.25	10.26	16.67	11.10	31.21	1.41	-0.65	-60	0.00	-56.21	-46.27	-46.90	56.21
11.489	50.66	11.49	18.40	11.74	34.45	1.58	-0.87	-70	-0.00	-62.73	-53.02	-56.90	62.73
12.730	56.13	12.73	20.13	12.36	37.68	1.75	-1.10	-80	-0.00	-69.30	-59.78	-66.90	69.30



Pressure Drop 2 to 3 [mmHg]	Pressure Drop 3 to 4 [mmHg]	Total Pressure Drop [mmHg]	Shear Stress 1 to 2 [dynes/cm <sup>2</sup> ]	Shear Stress 2 to 3 [dynes/cm <sup>2</sup> ]	Shear Stress 3 to 4 [dynes/cm <sup>2</sup> ]
-13.05	-18.76	-13	147.37	26.96	78.16
-12.23	-15.56	-3	194.41	25.26	64.81
-11.57	-12.34	7	242.57	23.89	51.38
-11.03	-9.10	17	291.62	22.78	37.92
-10.59	-5.86	27	341.38	21.87	24.42
-10.23	-2.62	37	391.75	21.13	10.91
-9.94	0.63	47	442.64	20.52	2.61
-9.71	3.87	57	493.97	20.04	16.14
-9.52	7.12	67	545.71	19.66	29.66



$V_0 E^2/2g$	$h_{in}$	$h_{out}$	$h_{1/A,B}$	$h_{1/C,D}$	$h_{1/D,E}$	$h_{diverg, flow}$	$h_{converg, flow}$	Cardiotomy Pressure mmHg	$P_1$ [mmHg]	$P_2$ [mmHg]	$P_3$ [mmHg]	$P_4$ [mmHg]	Pressure Drop 1 to 2 [mmHg]
3.106	16.70	3.11	9.47	6.10	6.05	1.06	0.67	0	-0.00	-24.18	-10.08	13.10	24.18
3.667	19.72	3.67	10.95	6.63	12.68	1.26	0.57	-10	-0.00	-28.36	-14.58	3.10	28.36
4.597	24.72	4.60	13.34	7.43	15.46	1.58	0.40	-20	-0.00	-35.26	-21.87	-6.90	35.26
5.549	29.84	5.55	15.73	8.16	18.22	1.90	0.22	-30	-0.00	-42.27	-29.15	-16.90	42.27
6.519	35.05	6.52	18.11	8.84	20.98	2.23	0.04	-40	0.00	-49.37	-36.44	-26.90	49.37
7.503	40.35	7.50	20.48	9.49	23.73	2.57	-0.14	-50	0.00	-56.54	-43.72	-36.90	56.54
8.500	45.71	8.50	22.85	10.10	26.47	2.91	-0.32	-60	0.00	-63.78	-51.00	-46.90	63.78
9.509	51.13	9.51	25.20	10.68	29.19	3.26	-0.51	-70	-0.00	-71.07	-58.28	-56.90	71.07
10.528	56.61	10.53	27.55	11.24	31.91	3.61	-0.69	-80	-0.00	-78.41	-65.56	-66.90	78.41

Pressure Drop 2 to 3 [mmHg]	Pressure Drop 3 to 4 [mmHg]	Total Pressure Drop [mmHg]	Shear Stress 1 to 2 [dynes/cm <sup>2</sup> ]	Shear Stress 2 to 3 [dynes/cm <sup>2</sup> ]	Shear Stress 3 to 4 [dynes/cm <sup>2</sup> ]
-14.10	-23.18	-13	178.78	29.12	96.54
-13.79	-17.68	-3	209.76	28.47	73.64
-13.40	-14.97	7	260.79	27.66	62.36
-13.12	-12.26	17	312.62	27.09	51.05
-12.94	-9.54	27	365.12	26.71	39.73
-12.83	-6.82	37	418.17	26.49	28.41
-12.78	-4.10	47	471.69	26.40	17.08
-12.79	-1.38	57	525.61	26.42	5.76
-12.85	1.33	67	579.90	26.54	5.56



Reynold's # 3.4	Reynold's # 4.5	z-density/g	V <sub>svc</sub> <sup>2</sup> /2g	V <sub>vc</sub> <sup>2</sup> /2g	V <sub>svc</sub> cannuas <sup>2</sup> /2g	V <sub>vc</sub> cannuas <sup>2</sup> /2g	V <sub>i</sub> <sup>2</sup> /2g	V <sub>i</sub> <sup>2</sup> /2g	V <sub>i</sub> <sup>2</sup> /2g	h <sub>svc</sub>	h <sub>vc</sub>	h <sub>out</sub>	h <sub>svc</sub> cannuas	h <sub>vc</sub> cannuas	h <sub>svc</sub> line	h <sub>vc</sub> line	h <sub>conwsg</sub> flow 2.4	h <sub>conwsg</sub> flow 3.4	h <sub>4.5</sub>
1271	2542	17469.648	0.037	0.037	4.617	4.617	0.727	0.727	2.908	16.78	16.78	2.91	12.44	12.44	5.91	5.91	0.71	0.71	10.42
1454	2908	17469.648	0.049	0.049	6.040	6.040	0.951	0.951	3.804	21.96	21.96	3.80	15.74	15.74	6.76	6.76	0.54	0.54	13.18
1619	3239	17469.648	0.061	0.061	7.494	7.494	1.180	1.180	4.720	27.24	27.24	4.72	19.01	19.01	7.53	7.53	0.37	0.37	15.92
1772	3544	17469.648	0.073	0.073	8.974	8.974	1.413	1.413	5.652	32.62	32.62	5.65	22.26	22.26	8.23	8.23	0.20	0.20	18.64
1914	3829	17469.648	0.085	0.085	10.474	10.474	1.649	1.649	6.597	38.08	38.08	6.60	25.46	25.46	8.90	8.90	0.03	0.03	21.34
2048	4097	17469.648	0.097	0.097	11.992	11.992	1.888	1.888	7.553	43.60	43.60	7.55	28.69	28.69	9.52	9.52	-0.15	-0.15	24.02
2176	4351	17469.648	0.110	0.110	13.527	13.527	2.130	2.130	8.519	49.17	49.17	8.52	31.87	31.87	10.11	10.11	-0.33	-0.33	26.69
2297	4593	17469.648	0.122	0.122	15.075	15.075	2.374	2.374	9.494	54.80	54.80	9.49	35.05	35.05	10.67	10.67	-0.50	-0.50	29.35
2413	4825	17469.648	0.135	0.135	16.635	16.635	2.619	2.619	10.477	60.48	60.48	10.48	38.20	38.20	11.21	11.21	-0.69	-0.69	31.99

hda, change SVC cannula-2	hda, change IVC cannula-3	Cardiotomy Pressure Pc [mmHg]	Pvc [mmHg]	P2 [mmHg]	P3 [mmHg]	P4 [mmHg]	P5 [mmHg]	Pressure Drop SVC to 2 [mmHg]	Pressure Drop IVC to 3 [mmHg]	Pressure Drop 2 to 4 [mmHg]
0.07	0.07	0	-0.00	-23.39	-23.39	-8.49	13.10	23.39	23.39	-14.90
0.09	0.09	-10	-0.00	-30.18	-30.18	-16.33	3.10	30.18	30.18	-13.84
0.11	0.11	-20	0.00	-37.03	-37.03	-24.20	-6.90	37.03	37.03	-12.84
0.13	0.13	-30	-0.00	-43.95	-43.95	-32.08	-16.90	43.95	43.95	-11.87
0.15	0.15	-40	-0.00	-50.91	-50.91	-39.97	-26.90	50.91	50.91	-10.94
0.17	0.17	-50	0.00	-57.91	-57.91	-47.88	-36.90	57.91	57.91	-10.03
0.20	0.20	-60	0.00	-64.94	-64.94	-55.80	-46.90	64.94	64.94	-9.15
0.22	0.22	-70	0.00	-72.00	-72.00	-63.73	-56.90	72.00	72.00	-8.28
0.24	0.24	-80	0.00	-79.09	-79.09	-71.66	-66.90	79.09	79.09	-7.42

Pressure Drop 3 to 4 [mmHg]	Pressure Drop 4 to 5 [mmHg]	Total Pressure Drop [mmHg]	Shear Stress SVC to 2 [dynes/cm <sup>2</sup> ]	Shear Stress IVC to 3 [dynes/cm <sup>2</sup> ]	Shear Stress 2 to 4 [dynes/cm <sup>2</sup> ]	Shear Stress 3 to 4 [dynes/cm <sup>2</sup> ]	Shear Stress 4 to 5 [dynes/cm <sup>2</sup> ]
-14.90	-21.59	-13.10	138.32	136.32	30.77	30.77	89.33
-13.84	-19.43	-3.10	175.89	175.89	28.59	28.59	80.42
-12.84	-17.30	6.90	215.88	215.88	26.51	26.51	71.56
-11.87	-15.18	16.90	256.19	256.19	24.52	24.52	62.81
-10.94	-13.07	26.90	296.76	296.76	22.59	22.59	54.09
-10.03	-10.98	36.90	337.56	337.56	20.72	20.72	45.43
-9.15	-8.90	46.90	378.54	378.54	18.89	18.89	36.82
-8.28	-6.83	56.90	419.69	419.69	17.09	17.09	28.25
-7.42	-4.77	66.90	460.99	460.99	15.33	15.33	19.73



**18 Fr. Single-Stage cannula:**

SVC Diameter [cm]:	2	SVC Flow [cm³/s]	19.8	IVCFlow [cm³/s]	19.8	Vsvc [cm/s]	6.31	Vivc [cm/s]	6.31	Vsvc cannula [cm/s]	124.61	Vivc cannula [cm/s]	124.61	V2 [cm/s]	27.81	V3 [cm/s]	27.81	V4 [cm/s]	55.63	Reynold's # SVC Cannula	1981	Reynold's # IVC Cannula	1981	Reynold's # 2.4	936
IVC Diameter [cm]:	2		22.8		22.8	7.26	7.26	7.26	7.26	143.50	143.50	143.50	143.50	32.03	32.03	32.03	32.03	64.06	2282	2282	2282	1078			
SVC Area [cm²]	3.14		25.6		25.6	8.13	8.13	8.13	8.13	160.89	160.89	160.89	160.89	35.87	35.87	35.87	35.87	71.73	2555	2555	2555	1207			
IVC Area [cm²]	3.14		27.2		27.2	8.65	8.65	8.65	8.65	170.95	170.95	170.95	170.95	38.16	38.16	38.16	38.16	76.31	2718	2718	2718	1284			
SVC Cannula ID [cm]:	0.45		29.4		29.4	9.36	9.36	9.36	9.36	184.93	184.93	184.93	184.93	41.28	41.28	41.28	41.28	82.55	2940	2940	2940	1389			
IVC Cannula ID [cm]:	0.45		31.5		31.5	10.03	10.03	10.03	10.03	198.11	198.11	198.11	198.11	44.22	44.22	44.22	44.22	88.44	3150	3150	3150	1488			
Venous Line Diameter [cm]:	0.9525		33.5		33.5	10.66	10.66	10.66	10.66	210.64	210.64	210.64	210.64	47.01	47.01	47.01	47.01	94.03	3349	3349	3349	1582			
Diameter 4.5 [cm]:	0.9525		35.4		35.4	11.27	11.27	11.27	11.27	222.60	222.60	222.60	222.60	49.68	49.68	49.68	49.68	99.37	3539	3539	3539	1672			
SVC Cannula Area [cm²]:	0.159		37.2		37.2	11.85	11.85	11.85	11.85	234.07	234.07	234.07	234.07	52.24	52.24	52.24	52.24	104.48	3722	3722	3722	1758			
IVC Cannula Area [cm²]:	0.159																								
Venous Line Area [cm²]:	0.713																								
Area 4.5 [cm²]:	0.713																								
Viscosity [g/cm·s]:	0.03																								
Density [g/cm3]:	1.06																								
Acc. due to gravity [cm/s²]:	981																								
Specific weight [g/s²·cm²]:	1039.9																								
Cannula Length [cm]:	34																								
Length CD [cm]:	153.7																								
Length DE [cm]:	76.7																								
Height Zsvc,ivc [cm]:	66																								
Height Za3 [cm]:	66																								
Height Za [cm]:	38.1																								
Height Zc [cm]:	16.8																								
Ki,cat:	1																								
Ki,inf:	1.33																								
Ki,expansion:	0.04																								
Convergence angle, β [degrees]:	30																								
Convergence angle, β' [degrees]:	36.954																								
Converging coefficient, μ3:	0.96																								
Flow [L/min]	2.37																								

[illegible]

hda: change SVC catheter-2	hda: change IVC catheter-3	Cardiotomy Pressure Pc [mmHg]	Pvc [mmHg]	P2 [mmHg]	P3 [mmHg]	P4 [mmHg]	P5 [mmHg]	Pressure Drop SVC to 2 [mmHg]	Pressure Drop IVC to 3 [mmHg]	Pressure Drop 2 to 4 [mmHg]
0.19	0.19	0	0.00	-29.93	-29.93	-13.23	13.10	29.93	29.93	-16.70
0.25	0.25	-10	-0.00	-38.68	-38.68	-22.71	3.10	38.68	38.68	-15.96
0.32	0.32	-20	0.00	-47.51	-47.51	-32.25	-8.90	47.51	47.51	-15.26
0.36	0.36	-30	0.00	-53.17	-53.17	-38.34	-16.90	53.17	53.17	-14.83
0.42	0.42	-40	0.00	-61.34	-61.34	-47.12	-26.90	61.34	61.34	-14.22
0.48	0.48	-50	0.00	-69.54	-69.54	-55.90	-36.90	69.54	69.54	-13.84
0.55	0.55	-60	0.00	-77.76	-77.76	-64.69	-46.90	77.76	77.76	-13.07
0.61	0.61	-70	0.00	-85.99	-85.99	-73.48	-56.90	85.99	85.99	-12.51
0.67	0.67	-80	0.00	-94.23	-94.23	-82.27	-66.90	94.23	94.23	-11.96

Pressure Drop 3 to 4 [mmHg]	Pressure Drop 4 to 5 [mmHg]	Total Pressure Drop [mmHg]	Shear Stress SVC to 2 [dynes/cm <sup>2</sup> ]	Shear Stress IVC to 3 [dynes/cm <sup>2</sup> ]	Shear Stress 2 to 4 [dynes/cm <sup>2</sup> ]	Shear Stress 3 to 4 [dynes/cm <sup>2</sup> ]	Shear Stress 4 to 5 [dynes/cm <sup>2</sup> ]
-16.70	-26.33	-13.10	132.00	132.00	34.49	34.49	108.95
-15.86	-25.82	-3.10	170.57	170.57	32.96	32.96	106.83
-15.28	-25.35	6.90	209.52	209.52	31.51	31.51	104.80
-14.83	-21.44	16.90	234.48	234.48	30.62	30.62	88.72
-14.22	-20.22	26.90	270.54	270.54	28.37	28.37	83.67
-13.64	-19.00	36.90	306.69	306.69	28.16	28.16	78.64
-13.07	-17.79	46.90	342.93	342.93	26.99	26.99	73.62
-12.51	-16.56	56.90	379.24	379.24	25.83	25.83	68.61
-11.96	-15.37	66.90	415.61	415.61	24.70	24.70	63.62



[illegible]

hds change SVC cannula-2	hds change IVC cannula-3	Cardiotomy Pressure Pc [mmHg]	Pvc [mmHg]	Pvc [mmHg]	P2 [mmHg]	P3 [mmHg]	P4 [mmHg]	P5 [mmHg]	Pressure Drop SVC to 2 [mmHg]	Pressure Drop IVC to 3 [mmHg]	Pressure Drop 2 to 4 [mmHg]
0.17	0.17	0	0.00	0.00	-35.70	-35.70	-15.78	13.10	35.70	35.70	-19.92
0.28	0.28	-10	-0.00	-0.00	-45.24	-45.24	-25.56	3.10	45.24	45.24	-19.68
0.40	0.40	-20	-0.00	-0.00	-54.78	-54.78	-35.35	-6.90	54.78	54.78	-19.43
0.55	0.55	-30	-0.00	-0.00	-64.32	-64.32	-45.14	-16.90	64.32	64.32	-19.19
0.71	0.71	-40	-0.00	-0.00	-73.87	-73.87	-54.93	-26.90	73.87	73.87	-18.94
0.90	0.90	-50	0.00	0.00	-83.41	-83.41	-64.72	-36.90	83.41	83.41	-18.68
1.10	1.10	-60	-0.00	-0.00	-92.95	-92.95	-74.52	-46.90	92.95	92.95	-18.43
1.32	1.32	-70	-0.00	-0.00	-102.49	-102.49	-84.32	-56.90	102.49	102.49	-18.17
1.56	1.56	-80	0.00	0.00	-112.03	-112.03	-94.12	-66.90	112.03	112.03	-17.92

Pressure Drop 3 to 4 [mmHg]	Pressure Drop 4 to 5 [mmHg]	Total Pressure Drop [mmHg]	Shear Stress SVC to 2 [dynes/cm <sup>2</sup> ]	Shear Stress IVC to 3 [dynes/cm <sup>2</sup> ]	Shear Stress 2 to 4 [dynes/cm <sup>2</sup> ]	Shear Stress 3 to 4 [dynes/cm <sup>2</sup> ]	Shear Stress 4 to 5 [dynes/cm <sup>2</sup> ]
-19.92	-28.88	-13.10	97.50	97.50	41.13	41.13	119.52
-19.68	-28.67	-3.10	123.57	123.57	40.63	40.63	118.63
-19.43	-28.45	6.90	149.63	149.63	40.13	40.13	117.74
-19.19	-28.24	16.90	175.69	175.69	39.62	39.62	116.87
-18.94	-28.03	26.90	201.76	201.76	39.10	39.10	116.01
-18.68	-27.83	36.90	227.82	227.82	38.58	38.58	115.15
-18.43	-27.62	46.90	253.88	253.88	38.06	38.06	114.31
-18.17	-27.42	56.90	279.94	279.94	37.53	37.53	113.47
-17.92	-27.22	66.90	306.00	306.00	37.00	37.00	112.64



**Appendix G:**  
Statistical Powers for the Analysis of the Bubble Count Data of  
Each Cannula

Cannula	Statistical Power
28/38 Fr. Dual-Stage Cannula	0.44
29/29 Fr. Dual-Stage Cannula	0.79
24 Fr. Single-Stage Cannula	0.61
18 Fr. Single-Stage Cannula	0.08
12 Fr. Single-Stage Cannula	0.06

**Appendix H:**  
t-Statistic Calculation for the Comparison of the Model and  
Measured Data

Cannula	Vacuum	Measured Flow	squared values	Predicted Flow	Estimated Wall Shear Stress	squared values	Predicted Wall Shear Stress
1	1	3.45	11.9025	3.48	94.5	8930.25	122.26
1	1	3.43	11.7649	3.48	86.62	7503.0244	122.26
1	1	3.41	11.6281	3.48	94.5	8930.25	122.26
1	1	3.44	11.8336	3.48	94.5	8930.25	122.26
1	1	3.41	11.6281	3.48	86.62	7503.0244	122.26
1	2	4.25	18.0625	4.02	133.87	17921.1769	165.92
1	2	4	16	4.02	118.12	13952.3344	165.92
1	2	3.97	15.7609	4.02	118.12	13952.3344	165.92
1	2	4.02	16.1604	4.02	118.12	13952.3344	165.92
1	2	4.01	16.0801	4.02	110.25	12155.0625	165.92
1	3	4.66	21.7156	4.49	102.37	10479.6169	211.79
1	3	4.5	20.25	4.49	149.62	22386.1444	211.79
1	3	4.53	20.5209	4.49	149.62	22386.1444	211.79
1	3	4.47	19.9809	4.49	141.74	20090.2276	211.79
1	3	4.48	20.0704	4.49	141.74	20090.2276	211.79
1	4	4.9	24.01	4.92	165.37	27347.2369	259.55
1	4	4.98	24.8004	4.92	173.24	30012.0976	259.55
1	4	4.97	24.7009	4.92	173.24	30012.0976	259.55
1	4	4.92	24.2064	4.92	173.24	30012.0976	259.55
1	4	4.93	24.3049	4.92	165.37	27347.2369	259.55
1	5	5	25	5.31	94.5	8930.25	308.97
1	5	5.35	28.6225	5.31	188.99	35717.2201	308.97
1	5	5.41	29.2681	5.31	204.74	41918.4676	308.97
1	5	5.4	29.16	5.31	196.87	38757.7969	308.97
1	5	5.29	27.9841	5.31	196.87	38757.7969	308.97
1	6	5.68	32.2624	5.67	220.49	48615.8401	359.88
1	6	5.69	32.3761	5.67	228.37	52152.8569	359.88
1	6	5.73	32.8329	5.67	220.49	48615.8401	359.88
1	6	5.7	32.49	5.67	228.37	52152.8569	359.88
1	6	5.69	32.3761	5.67	220.49	48615.8401	359.88
1	7	5.86	34.3396	6	228.37	52152.8569	412.13
1	7	5.91	34.9281	6	228.37	52152.8569	412.13
1	7	5.98	35.7604	6	236.24	55809.3376	412.13
1	7	5.97	35.6409	6	236.24	55809.3376	412.13
1	7	6.01	36.1201	6	244.12	59594.5744	412.13
1	8	6.43	41.3449	6.31	228.37	52152.8569	465.6
1	8	6.3	39.69	6.31	259.87	67532.4169	465.6
1	8	6.28	39.4384	6.31	251.99	63498.9601	465.6
1	8	6.32	39.9424	6.31	259.87	67532.4169	465.6
1	8	6.26	39.1876	6.31	251.99	63498.9601	465.6
1	9	6.49	42.1201	6.59	267.74	71684.7076	520.21
1	9	6.61	43.6921	6.59	267.74	71684.7076	520.21
1	9	6.62	43.8244	6.59	283.49	80366.5801	520.21
1	9	6.59	43.4281	6.59	259.87	67532.4169	520.21
1	9	6.58	43.2964	6.59	275.62	75966.3844	520.21
2	1	3.06	9.3636	3.21	118.33	14001.9889	155.26
2	1	3.05	9.3025	3.21	125.72	15805.5184	155.26
2	1	3.11	9.6721	3.21	118.33	14001.9889	155.26
2	1	3.06	9.3636	3.21	125.72	15805.5184	155.26
2	2	3.59	12.8881	3.56	147.91	21877.3681	187.19
2	2	3.65	13.3225	3.56	147.91	21877.3681	187.19
2	2	3.67	13.4689	3.56	147.91	21877.3681	187.19
2	2	3.56	12.6736	3.56	147.91	21877.3681	187.19
2	2	3.57	12.7449	3.56	147.91	21877.3681	187.19
2	3	4.06	16.4836	4.01	177.49	31502.7001	233.96
2	3	4.1	16.81	4.01	177.49	31502.7001	233.96
2	3	4.12	16.9744	4.01	184.88	34180.6144	233.96
2	3	4.06	16.4836	4.01	184.88	34180.6144	233.96
2	3	4.04	16.3216	4.01	177.49	31502.7001	233.96
2	4	4.52	20.4304	4.44	207.07	42877.9849	281.36
2	4	4.56	20.7936	4.44	207.07	42877.9849	281.36
2	4	4.39	19.2721	4.44	207.07	42877.9849	281.36
2	4	4.51	20.3401	4.44	207.07	42877.9849	281.36
2	4	4.5	20.25	4.44	207.07	42877.9849	281.36
2	5	4.86	23.6196	4.84	236.65	56003.2225	329.22
2	5	4.94	24.4036	4.84	236.65	56003.2225	329.22
2	5	5.01	25.1001	4.84	244.05	59560.4025	329.22
2	5	4.88	23.8144	4.84	236.65	56003.2225	329.22
2	5	4.87	23.7169	4.84	236.65	56003.2225	329.22
2	6	5.34	28.5156	5.22	266.23	70878.4129	377.42
2	6	5.3	28.09	5.22	266.23	70878.4129	377.42
2	6	5.34	28.5156	5.22	273.63	74873.3769	377.42
2	6	5.29	27.9841	5.22	266.23	70878.4129	377.42
2	6	5.28	27.8784	5.22	273.63	74873.3769	377.42

2	7	5.58	31.1364	5.59	295.81	87503.5561	425.86
2	7	5.59	31.2481	5.59	273.63	74873.3769	425.86
2	7	5.64	31.8096	5.59	303.21	91936.3041	425.86
2	7	5.59	31.2481	5.59	295.81	87503.5561	425.86
2	7	5.65	31.9225	5.59	303.21	91936.3041	425.86
2	8	5.83	33.9889	5.94	310.6	96472.36	474.49
2	8	5.88	34.5744	5.94	318	101124	474.49
2	8	5.87	34.4569	5.94	318	101124	474.49
2	8	5.82	33.8724	5.94	310.6	96472.36	474.49
2	8	5.83	33.9889	5.94	325.39	105878.6521	474.49
2	9	6.14	37.6996	6.28	332.79	110749.1841	523.23
2	9	6.18	38.1924	6.28	340.19	115729.2361	523.23
2	9	6.15	37.8225	6.28	340.19	115729.2361	523.23
2	9	6.14	37.6996	6.28	332.79	110749.1841	523.23
2	9	6.2	38.44	6.28	340.19	115729.2361	523.23
3	1	0.66	0.4356	0.61	86.04	7402.8816	96.49
3	1	0.67	0.4489	0.61	81.94	6714.1636	96.49
3	1	0.67	0.4489	0.61	83.31	6940.5561	96.49
3	1	0.66	0.4356	0.61	84.67	7169.0089	96.49
3	1	0.67	0.4489	0.61	83.31	6940.5561	96.49
3	2	0.78	0.6084	0.79	102.43	10491.9049	122.11
3	2	0.78	0.6084	0.79	103.79	10772.3641	122.11
3	2	0.79	0.6241	0.79	106.52	11346.5104	122.11
3	2	0.79	0.6241	0.79	105.16	11058.6256	122.11
3	2	0.79	0.6241	0.79	103.79	10772.3641	122.11
3	3	0.88	0.7744	0.95	125.64	15785.4096	147.84
3	3	0.9	0.81	0.95	124.28	15445.5184	147.84
3	3	0.9	0.81	0.95	124.28	15445.5184	147.84
3	3	0.89	0.7921	0.95	124.28	15445.5184	147.84
3	3	0.9	0.81	0.95	125.64	15785.4096	147.84
3	4	1.04	1.0816	1.09	148.86	22159.2996	173.78
3	4	1.05	1.1025	1.09	152.96	23396.7616	173.78
3	4	1.02	1.0404	1.09	148.86	22159.2996	173.78
3	4	1.03	1.0609	1.09	151.59	22979.5281	173.78
3	4	1.05	1.1025	1.09	151.59	22979.5281	173.78
3	5	1.13	1.2769	1.21	169.34	28676.0356	199.96
3	5	1.13	1.2769	1.21	170.71	29141.9041	199.96
3	5	1.14	1.2996	1.21	170.71	29141.9041	199.96
3	5	1.14	1.2996	1.21	169.34	28676.0356	199.96
3	5	1.13	1.2769	1.21	169.34	28676.0356	199.96
3	6	1.24	1.5376	1.3	188.46	35517.1716	226.37
3	6	1.28	1.6384	1.3	195.29	38138.1841	226.37
3	6	1.24	1.5376	1.3	189.83	36035.4289	226.37
3	6	1.26	1.5876	1.3	191.19	36553.6161	226.37
3	6	1.25	1.5625	1.3	191.19	36553.6161	226.37
3	7	1.37	1.8769	1.37	214.41	45971.6481	252.96
3	7	1.37	1.8769	1.37	215.78	46561.0084	252.96
3	7	1.36	1.8496	1.37	210.31	44230.2961	252.96
3	7	1.37	1.8769	1.37	211.68	44808.4224	252.96
3	7	1.36	1.8496	1.37	213.05	45390.3025	252.96
3	8	1.48	2.1904	1.43	240.36	57772.9296	279.71
3	8	1.45	2.1025	1.43	233.53	54536.2609	279.71
3	8	1.46	2.1316	1.43	240.36	57772.9296	279.71
3	8	1.47	2.1609	1.43	238.99	57116.2201	279.71
3	8	1.46	2.1316	1.43	236.26	55818.7876	279.71
3	9	1.57	2.4649	1.47	262.21	68754.0841	306.56
3	9	1.58	2.4964	1.47	266.31	70921.0161	306.56
3	9	1.56	2.4336	1.47	255.38	65218.9444	306.56
3	9	1.58	2.4964	1.47	262.21	68754.0841	306.56
3	9	1.57	2.4649	1.47	262.21	68754.0841	306.56
4	1	2.21	4.8841	2.37	97.03	9414.8209	127.03
4	1	2.21	4.8841	2.37	92.62	8578.4644	127.03
4	1	2.24	5.0176	2.37	92.62	8578.4644	127.03
4	1	2.22	4.9284	2.37	94.82	8990.8324	127.03
4	1	2.23	4.9729	2.37	92.62	8578.4644	127.03
4	2	2.58	6.6564	2.57	116.87	13658.5969	167.73
4	2	2.57	6.6049	2.57	112.46	12647.2516	167.73
4	2	2.65	7.0225	2.57	121.28	14708.8384	167.73
4	2	2.63	6.9169	2.57	114.67	13149.2089	167.73
4	2	2.58	6.6564	2.57	121.28	14708.8384	167.73
4	3	2.96	8.7616	2.93	136.72	18692.3584	205.37
4	3	2.95	8.7025	2.93	143.34	20546.3556	205.37
4	3	2.97	8.8209	2.93	141.13	19917.6769	205.37
4	3	2.95	8.7025	2.93	141.13	19917.6769	205.37
4	3	2.97	8.8209	2.93	143.34	20546.3556	205.37
4	4	3.32	11.0224	3.21	167.59	28086.4081	231.19
4	4	3.24	10.4976	3.21	165.39	27353.8521	231.19

4	4	3.32	11.0224	3.21	165.39	27353.8521	231.19
4	4	3.28	10.7584	3.21	165.39	27353.8521	231.19
4	4	3.33	11.0889	3.21	165.39	27353.8521	231.19
4	5	3.74	13.9876	3.54	194.05	37655.4025	264.56
4	5	3.61	13.0321	3.54	189.64	35963.3296	264.56
4	5	3.65	13.3225	3.54	191.85	36806.4225	264.56
4	5	3.62	13.1044	3.54	191.85	36806.4225	264.56
4	5	3.71	13.7641	3.54	189.64	35963.3296	264.56
4	6	3.93	15.4449	3.88	220.52	48629.0704	297.18
4	6	3.96	15.6816	3.88	220.52	48629.0704	297.18
4	6	3.92	15.3664	3.88	216.11	46703.5321	297.18
4	6	3.95	15.6025	3.88	222.72	49604.1984	297.18
4	6	3.94	15.5236	3.88	218.31	47659.2561	297.18
4	7	4.28	18.3184	4.23	249.18	62090.6724	328.88
4	7	4.26	18.1476	4.23	249.18	62090.6724	328.88
4	7	4.25	18.0625	4.23	246.98	60999.1204	328.88
4	7	4.25	18.0625	4.23	246.98	60999.1204	328.88
4	7	4.25	18.0625	4.23	246.98	60999.1204	328.88
4	8	4.46	19.8916	4.58	271.24	73571.1376	359.49
4	8	4.6	21.16	4.58	280.06	78433.6036	359.49
4	8	4.47	19.9809	4.58	271.24	73571.1376	359.49
4	8	4.49	20.1601	4.58	277.85	77200.6225	359.49
4	8	4.5	20.25	4.58	275.65	75982.9225	359.49
4	9	4.74	22.4676	4.96	297.7	88625.29	388.78
4	9	4.76	22.6576	4.96	297.7	88625.29	388.78
4	9	4.79	22.9441	4.96	302.11	91270.4521	388.78
4	9	4.75	22.5625	4.96	299.9	89940.01	388.78
4	9	4.78	22.8484	4.96	302.11	91270.4521	388.78
5	1	3.03	9.1809	3.1	81.61	6660.1921	135.08
5	1	3.11	9.6721	3.1	84.52	7143.6304	135.08
5	1	3.1	9.61	3.1	81.61	6660.1921	135.08
5	1	3.09	9.5481	3.1	84.52	7143.6304	135.08
5	1	3.05	9.3025	3.1	84.52	7143.6304	135.08
5	2	3.57	12.7449	3.58	102.01	10406.0401	173.24
5	2	3.54	12.5316	3.58	104.92	11008.2064	173.24
5	2	3.61	13.0321	3.58	110.75	12265.5625	173.24
5	2	3.53	12.4609	3.58	104.92	11008.2064	173.24
5	2	3.48	12.1104	3.58	99.09	9818.8281	173.24
5	3	4.05	16.4025	4.02	122.41	14984.2081	211.2
5	3	4.04	16.3216	4.02	128.24	16445.4976	211.2
5	3	4.03	16.2409	4.02	125.32	15705.1024	211.2
5	3	4.05	16.4025	4.02	128.24	16445.4976	211.2
5	3	4.05	16.4025	4.02	128.24	16445.4976	211.2
5	4	4.51	20.3401	4.45	151.55	22967.4025	248.82
5	4	4.45	19.8025	4.45	142.81	20394.6961	248.82
5	4	4.53	20.5209	4.45	151.55	22967.4025	248.82
5	4	4.47	19.9809	4.45	148.64	22093.8496	248.82
5	4	4.44	19.7136	4.45	148.64	22093.8496	248.82
5	5	4.93	24.3049	4.86	171.96	29570.2416	285.99
5	5	4.84	23.4256	4.86	171.96	29570.2416	285.99
5	5	4.86	23.6196	4.86	171.96	29570.2416	285.99
5	5	4.87	23.7169	4.86	171.96	29570.2416	285.99
5	5	4.94	24.4036	4.86	169.04	28574.5216	285.99
5	6	5.26	27.6676	5.26	192.36	37002.3696	322.61
5	6	5.32	28.3024	5.26	195.27	38130.3729	322.61
5	6	5.3	28.09	5.26	198.19	39279.2761	322.61
5	6	5.31	28.1961	5.26	195.27	38130.3729	322.61
5	6	5.31	28.1961	5.26	195.27	38130.3729	322.61
5	7	5.68	32.2624	5.65	221.5	49062.25	358.6
5	7	5.56	30.9136	5.65	212.76	45266.8176	358.6
5	7	5.7	32.49	5.65	221.5	49062.25	358.6
5	7	5.65	31.9225	5.65	218.59	47781.5881	358.6
5	7	5.63	31.6969	5.65	218.59	47781.5881	358.6
5	8	5.97	35.6409	6.03	230.25	53015.0625	393.87
5	8	6.1	37.21	6.03	244.82	59936.8324	393.87
5	8	6.01	36.1201	6.03	241.9	58515.61	393.87
5	8	6.07	36.8449	6.03	244.82	59936.8324	393.87
5	8	5.89	34.6921	6.03	230.25	53015.0625	393.87
5	9	6.4	40.96	6.41	268.13	71893.6969	428.33
5	9	6.43	41.3449	6.41	262.31	68806.5361	428.33
5	9	6.31	39.8161	6.41	256.48	65781.9904	428.33
5	9	6.33	40.0689	6.41	262.31	68806.5361	428.33
5	9	6.28	39.4384	6.41	259.39	67283.1721	428.33
Sum		877.93	4098.7099	Sum	43128.29	9290812.319	
Sum^2/n		3425.604822		Sum^2/n	8266886.215		
Difference		673.1050782		Difference	1023926.104		

sb2 9.86012E-06  
sb 0.003140083

t (slope=1) -0.721964335  
t (slope=0) 317.7409174

t crit (95%) 1.645

**Results**

t (slope=1) non-sig diff in slopes  
t (slope=0) sig. Diff. In slopes

sb2 0.000678281  
sb 0.026043829

t (slope=1) -17.01329569  
t (slope=0) 21.38351549

t crit (95%) 1.645

**Results**

t (slope=1) sig. Diff. In slopes  
t (slope=0) sig. Diff. In slopes

**Regression analysis on measured vs. predicted flow:**  
SUMMARY OUTPUT

Regression Statistics	
Multiple R	0.998899991
R Square	0.997801192
Adjusted R Square	0.997791332
Standard Error	0.081467167
Observations	225

ANOVA

	df	SS	MS	F	Significance F
Regression	1	671.6250497	671.6	101196	2.408E-298
Residual	223	1.480028535	0.007		
Total	224	673.1050782			

	Coefficients	Standard Error	t Stat	P-value	Lower 95%	Upper 95%	Lower 95%	Upper 95%
Intercept	0.005652997	0.013398209	0.422	0.6735	-0.020750275	0.0320563	-0.02075027	0.032056269
Predicted Flow	0.997732972	0.003136415	318.1	2E-298	0.991552175	1.0039138	0.991552175	1.003913769

**Regression analysis on measured vs. predicted wall shear stress:**  
SUMMARY OUTPUT

Regression Statistics	
Multiple R	0.921272666
R Square	0.848743326
Adjusted R Square	0.848065045
Standard Error	26.35355143
Observations	225

ANOVA

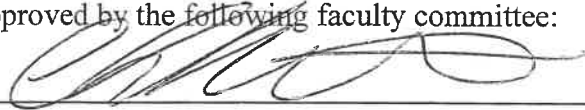
	df	SS	MS	F	Significance F
Regression	1	869050.4471	9E+05	1251.3	1.99867E-93
Residual	223	154875.657	694.5		
Total	224	1023926.104			

	Coefficients	Standard Error	t Stat	P-value	Lower 95%	Upper 95%	Lower 95.0%	Upper 95.0%
Intercept	36.39004023	4.728502018	7.696	5E-13	27.07178586	45.708295	27.07178586	45.7082946
Predicted Wall Shear Stress	0.556908629	0.015743475	35.37	2E-93	0.525883644	0.5879336	0.525883644	0.587933615



This research paper has been approved by the following faculty committee:

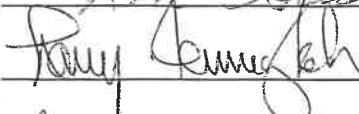
Faculty Chairperson:



Faculty:



Faculty:



Date:

June 5, 2000